

Key Points:

- Plagioclase deformation is revealed through micro-Raman, micro-infrared, and optical analyses of experimentally shocked basalts (0–63 GPa)
- Primary glass in basaltic andesite resulted in weaker spectral effects due to spectral similarities between glass and shocked plagioclase
- Onset of plagioclase amorphization in basalts occurs at comparable to slightly lower pressures to previous plagioclase-only experiments

Supporting Information:

- Supporting Information S1
- Data S1
- Data S2

Correspondence to:

J. R. Johnson,
jeffrey.r.johnson@jhuapl.edu

Citation:

Johnson, J. R., Jaret, S. J., Glotch, T. D., & Sims, M. (2020). Raman and infrared microspectroscopy of experimentally shocked basalts. *Journal of Geophysical Research: Planets*, 125, e2019JE006240. <https://doi.org/10.1029/2019JE006240>

Received 13 OCT 2019

Accepted 20 JAN 2020

Accepted article online 7 FEB 2020

Raman and Infrared Microspectroscopy of Experimentally Shocked Basalts

Jeffrey R. Johnson¹ , Steven J. Jaret² , Timothy D. Glotch³ , and Melissa Sims^{3,4} 

¹Johns Hopkins University Applied Physics Laboratory, Laurel, MD, USA, ²Department of Earth and Planetary Science, American Museum of Natural History, New York, NY, USA, ³Department of Geosciences, Stony Brook University, Stony Brook, NY, USA, ⁴Department of Earth and Planetary Sciences, Johns Hopkins University, Baltimore, MD, USA

Abstract Petrographic, micro-Raman and micro-Fourier transform infrared spectral analyses of experimentally shocked basalt and basaltic andesite samples (up to ~63 GPa) indicated that progressive amorphization of plagioclase feldspar with increasing pressure resulted in detectable spectral variations that mimic those of the experimentally shocked, plagioclase-dominated rocks analyzed in earlier studies.

However, variations in starting sample composition and/or shock propagation through the minerals and mesostasis within these basaltic rocks resulted in variable distribution of shock effects within the samples, as manifested in their infrared and Raman spectra. In particular, the presence of primary igneous glass within the starting samples subdued the observed effects because of the spectral similarity between the glass and shocked plagioclase (maskelynite and plagioclase glass). This caused ambiguity in distinguishing between amorphization resulting from shock effects and that associated with primary glass, particularly for the more hypocrySTALLINE basaltic andesite (~30% glass) compared to the basalt sample (~10% glass). Nonetheless, the correlation between shock pressures and key spectral parameters (Raman peak ratios, infrared reflectance peak band heights) for plagioclase-bearing sample areas terminated in the ~25–30 GPa pressure range. This was consistent with the amorphization onset pressures of andesine and reflected the increasing presence of maskelynite at these higher pressures. Higher spatial resolution mapping using these techniques could provide better insight regarding the influence of grain boundaries and mineralogical variations on shock propagation in fine-grained, glassy, basaltic samples. This would help refine the nature and magnitude of shock propagation effects in naturally shocked basaltic samples analyzed during in situ investigations of planetary surfaces.

Plain Language Summary During formation of an impact crater, minerals in rocks experience very high pressures that cause damage to their crystal structures. The primary mineral most easily changed by pressure is plagioclase feldspar, a common mineral in volcanic rocks (basalts) that occur on planetary surfaces. We used two basalts compressed to high shock pressures in the laboratory to analyze how their minerals changed with increasing pressure. We created thin slices of the shocked rocks and viewed their infrared reflectance and Raman spectra under a microscope to document the onset of formation of less crystalline, glassier materials that appeared at high pressures. Similar experiments were conducted previously on plagioclase minerals to document their changes at high pressures. The basaltic rocks analyzed here showed slightly more subdued changes compared to nearly monomineralic plagioclase samples, but overall trends were comparable. This was mainly due to the differences in glass content in the starting samples, because glasses share similar spectral shapes to highly shocked plagioclase. This ambiguity between impact-shocked materials and preexisting glass in volcanic rocks may complicate efforts to distinguish between the two when analyzing rocks with robotic instruments on planetary surfaces, but the techniques shown here demonstrate that such efforts would be valuable.

1. Introduction

Understanding the magnitude of shock pressures experienced during hypervelocity impact cratering events is a fundamental requirement for modeling impact processes on planetary surfaces, as well as a key component in recognizing impact-generated deposits (e.g., Melosh, 1989; Osinski & Pierazzo, 2013). Observations of pressure effects at the microscopic level can reveal important aspects of shock wave propagation through mineral grains and the resulting deformation to crystalline structures. Vibrational microspectroscopy using Raman and thermal infrared techniques provides a useful means to systematically analyze progressive

amorphization with pressure as manifested by variations in the position and magnitude of spectral features, particularly in plagioclase feldspars (Fritz et al., 2005, 2011; Heymann & Hörz, 1990; Jaret, Johnson, Sims, DiFrancesco, et al., 2018; Johnson et al., 2002). For example, plagioclase demonstrates progressive loss of complex spectral features with increasing pressure associated with Si–O bending and stretch vibrations in silica tetrahedra. Stronger, fourfold (tetrahedral) Si–Al coordination bonds transition to less polymerized, weaker bonds associated with sixfold (octahedral) coordination (e.g., Fritz et al., 2005; Johnson et al., 2002), to which both thermal infrared and Raman techniques are sensitive.

Jaret, Johnson, Sims, DiFrancesco, et al. (2018) used optical petrography, micro-Raman, and micro-Fourier transform infrared (FTIR) spectroscopy to document structural changes in experimentally shocked (0–56 GPa) albite-, andesine-, and bytownite-rich rocks as a function of composition and pressure (cf. Johnson, 2012; Johnson et al., 2002). They confirmed that sodic plagioclase samples began transformation to an amorphous phase at higher shock pressures than more calcic plagioclase. Average infrared reflectance spectra from two-dimensional (2-D) microscopic hyperspectral images of these samples mimicked emissivity measurements acquired previously on the bulk samples (Johnson, 2012; Johnson et al., 2002). However, heterogeneity in the shock response was observed on the microscopic scale. They suggested that the variability of the shock wave topology combined with differences in crystal orientation and composition were the likely causes.

Johnson et al. (2007) collected thermal infrared emission spectra of a suite of chips recovered from experimentally shocked (0–63 GPa) basalt (Grand Falls, AZ) and basaltic andesite (SP Flow, AZ) samples and documented variations in spectral features with increasing pressure that were consistent with deformation of the structure of plagioclase feldspars. Spectral features in the unshocked rocks arose from Si–O–Si octahedral bending vibrations ($350\text{--}700\text{ cm}^{-1}$) and Si–O antisymmetric stretch motions of the silica tetrahedra ($1,000\text{--}1,250\text{ cm}^{-1}$). These were altered at shock pressures $>20\text{--}25\text{ GPa}$ into two spectral features broadly near 960 and 400 cm^{-1} . Spectral unmixing models for the Grand Falls basalt shocked samples were improved by including shocked plagioclase spectra in the end-member libraries (Johnson et al., 2002, 2003). However, unshocked SP Flow basaltic andesite spectra were modeled erroneously using shocked feldspar spectra. Johnson et al. (2007) concluded that this was caused by the greater glass content of the basaltic andesite samples ($\sim 30\%$) compared to the Grand Falls basaltic samples ($\sim 10\%$).

Here we apply the microspectroscopy and petrographic techniques used by Jaret, Johnson, Sims, DiFrancesco, et al. (2018) on these shocked basaltic rocks to investigate systematically the structural damage induced by experimental shock processes within and among mineral grains and primary glasses at microscopic scales. Such information is relevant for laboratory spectral analyses of meteorites and naturally shocked terrestrial samples to better constrain shock pressure levels, as well as in the development and testing of in situ instruments on planetary spacecraft that would be capable of distinguishing impact shocked materials at high spatial resolution.

2. Background

2.1. Shock Experiments and Pressure Estimates

Previous petrographic investigations of experimentally and naturally shocked minerals attributed shock pressures to specific deformation features, the abundance of diaplectic glass, and variable degrees of melting (cf. Fritz et al., 2017; Grieve et al., 1996; Stöffler & Langenhorst, 1994; Thoma et al., 2005). These types of investigations have included samples ranging from meteorites (e.g., Stöffler et al., 1991, 2018; Bischoff & Stöffler, 1992; Cooney et al., 1999; Sharp & DeCarli, 2006; Gyollai et al., 2012; Rubin, 2015; Filiberto et al., 2018; Herd et al., 2017; Sharp et al., 2019; Chen et al., 2019) to lunar regolith samples (e.g., Fernandes et al., 2009, 2013; Hörz & Cintala, 1997; Pickersgill et al., 2015; Zeng et al., 2019) and terrestrial impact crater materials (e.g., Dence et al., 1977; Pickersgill, Osinski, & Flemming, 2015; Pickersgill, Flemming, & Osinski, 2015; Reimold, 1982; Short, 1970), all to better constrain their shock and thermal metamorphic histories. When plagioclase feldspars experience high pressures from impacts, disordering of the mineral lattice and increased abundance of amorphous phases typically occur at shock pressures above $\sim 20\text{ GPa}$ (Ahrens et al., 1969; Arndt et al., 1982; Bunch et al., 1967, 1968; Johnson, 2012; Lyon, 1963; Ostertag, 1983; Stöffler, 1971, 1972, 1974; Stöffler & Hornemann, 1972). Based on laboratory shock experiments, formation of maskelynite (diaplectic glass) from plagioclase is complete between ~ 30 and 45 GPa and significant

melting occurs at greater than ~ 45 GPa (Gibbons et al., 1975; Hörz & Cintala, 1997; Stöffler, 1972; Velde et al., 1987, 1989). For comparison, pyroxene and olivine are more resistant to the levels of shock pressure examined here, as was exemplified by no observed changes in thermal infrared spectra of experimentally shocked pyroxenes by Johnson et al. (2002) and by Raman spectroscopy for experimentally shocked olivines (Farrell-Turner et al., 2005; Harriss & Burchell, 2016).

The absolute strain rate, shock pulse duration, porosity, and initial temperature all influence the nature of the pressures experienced at the microscopic level by individual grains (Beck et al., 2005; DeCarli et al., 2002; Fritz et al., 2017; Hörz & Cintala, 1997; Sharp & DeCarli, 2006; Sims et al., 2019; Stöffler, 1972, 1974; Stöffler, 2001). At such scales, the reflection and rarefaction of shock waves across grain boundaries can cause inhomogeneous shock pressure distributions in small sample volumes (~ 1 cm³; e.g., Hanss et al., 1978) and variations in local shock intensities on the millimeter scale (Trepman, 2008). Along some mineral boundaries, local melting occurs at lower pressures than expected (e.g., Sazonova et al., 1996). Stöffler (2001) suggested that polycrystalline rocks with minerals of different shock impedance would likely experience such “local pressure peaks.” This is particularly important in localized shock veins (tens of microns across) concentrated along grain boundaries that occur at intermediate pressures as a result of heterogeneous pressure-induced heating (Fritz et al., 2017; Herd et al., 2017; Hirata et al., 2009; Kubo et al., 2010; Sharp et al., 2019).

2.2. Thermal Infrared Spectroscopy of Experimentally Shocked Samples

As shock pressures increase, diaplectic glasses can mutually exist with crystalline phases, resulting in changes to characteristic vibrational frequencies in the thermal infrared. As detailed in many spectroscopy investigations, bending vibrations near $400\text{--}550$ cm⁻¹ (Si–O–Al structures) are paired with weaker bending Si–O–Si absorptions near $450\text{--}700$ cm⁻¹, SiO₆ stretching vibrations near $750\text{--}850$ cm⁻¹, and Si–O antisymmetric stretch motions in the $900\text{--}1,200$ -cm⁻¹ region (Arndt et al., 1982; Bunch et al., 1967; Daniel et al., 1995, 1997; Heymann & Hörz, 1990; Iiishi et al., 1971; Ostertag, 1983; Stöffler & Hornemann, 1972; Velde et al., 1987; Williams, 1998; Williams & Jeanloz, 1988, 1989; Yamaguchi & Sekine, 2000).

Johnson et al. (2002, 2003) and Johnson (2012) acquired thermal infrared spectra ($5\text{--}40$ μm ; $250\text{--}2,000$ cm⁻¹) of experimentally shocked, nearly monomineralic rocks composed of bytownite (An₇₉), andesine (An_{36–46}), and albite (An₀₂) over peak pressures from ~ 15 to ~ 60 GPa. In unshocked bytownite prominent absorption bands were noted at $1,115$ and near 945 cm⁻¹ and weaker bands occurred near $500\text{--}650$ cm⁻¹. In unshocked albite sharper spectral features occurred at $1,010$, $1,040$, and $1,150$ cm⁻¹, whereas the positions of andesine spectral features were near $1,005$ and $1,145$ cm⁻¹. Spectral features related to Si–O bending and stretching vibrations in plagioclase feldspars were lost during the change to amorphous glass with increasing pressure. Only two major spectral features remained at the highest pressures: a band near $440\text{--}460$ cm⁻¹ (related to Si–O–Al bending vibrations) and Si–O stretch bands at $\sim 1,040$ cm⁻¹ (albite), $\sim 1,020$ cm⁻¹ (andesine), and ~ 960 cm⁻¹ (bytownite). The differences in Si–O stretch band positions are likely caused by the weaker Al–O bonds in Ca-rich plagioclase (e.g., Fritz et al., 2011; Johnson et al., 2003; Sazonova et al., 2007).

2.3. Raman Spectroscopy of High-Pressure Phases

Because Raman spectroscopy is also sensitive to molecular vibrational modes that are affected by crystal composition and lattice structure, it is a common method to study variability in minerals. Velde et al. (1989) used Raman spectra to study three feldspar compositions experimentally shocked from 21 to 54 GPa and noted the greatest resiliency of albite to shock pressure. Raman spectra of experimentally shocked ($24\text{--}40$ GPa) andesine (An₄₉) and oligoclase (An₁₉) from Heymann and Hörz (1990) exhibited a loss and/or broadening of several spectral bands with increasing pressure. At pressures greater than 30 GPa the transition to diaplectic glass resulted in the loss of the Si–O–Al stretch bands. Daniel et al. (1995) noted the appearance of a band near $1,000$ cm⁻¹ in the Raman spectrum of shocked anorthite. This was similar to the result of Freeman et al. (2008), who presented Raman spectra of a variety of plagioclase feldspars, including a shocked anorthite from lunar meteorite NWA 773 that showed broadening of band widths with pressure, consistent with partial conversion to maskelynite. Fritz et al. (2005) used Raman measurements to quantify shock effects in meteorites through detailed analyses of plagioclase and maskelynite. They demonstrated that the progression in shock pressures, as indicated by refractive index changes, can be matched to characteristic degradation of the Raman spectra. In their microspectroscopic analyses of shocked plagioclase, Jaret,

Table 1
Basaltic Rock Shock Recovery Experiment Samples

Grand Falls EIL no. ^a	Peak pressure (GPa)	Number of 2-D infrared images	SP flow EIL no. ^a	Peak pressure (GPa)	Number of 2-D infrared images
-	0	1	-	0	1
3377	17.4	3	3455	17.2	1
3378	24	3	3456	23.9	2
3442	26.7	1	3457	28.4	8
3379	29	2	3458	30.3	3
3380	30.4	7	3463	35	3
3381	33.5	2	3459	38.9	2
3390	40.9	1	3462	43.8	2
3383	46.4	3	3460	52.2	1
3382	52.3	2	3482	57.2	1 ^c
3485	56.2	1 ^b	3481	57.8	1 ^c
3483	57.3	1 ^b	3470	62	1 ^c
3469	59.8	3 ^b	3472	63	1 ^c
3465	60.6	3 ^b			

^aEIL no. (Running Flat Plate Accelerator experiment number in Experimental Impact Laboratory (EIL) at Johnson Space Center); cf. Johnson et al. (2007).

^bGrand Falls samples 3483 and 3485 were physically combined (average pressure 56.75 GPa), as were samples 3465 and 3469 (average pressure 60.2 GPa).

^cSP flow samples 3481 and 3482 were physically combined (average pressure 57.5 GPa), as were samples 3470 and 3472 (average pressure 62.5 GPa).

Johnson, Sims, DiFrancesco, et al. (2018) also documented the loss of spectral peaks associated with plagioclase and the development of broader peaks centered near 480–500 cm⁻¹ beginning at pressures above ~28 GPa.

2.4. Microspectroscopy

As a shock wave propagates along grain boundaries or within an individual grain, the pressure and temperature can vary locally. High spatial resolution spectroscopy can enable analysis at the grain scale of the spectral effects of pressures and shock propagation. This was shown effectively by Palomba et al. (2006), who acquired infrared bidirectional reflectance spectra (1.6–16.7 μm, 600–6,000 cm⁻¹) of the Martian meteorite Zagami at small spatial scales (20–400 μm) to characterize maskelynite's Christiansen Feature position (~1,247 cm⁻¹) and broad band at 950 cm⁻¹. Thin sections and pressed powders of meteorite samples have also been analyzed using transmission/absorption spectroscopy (e.g., Benedix & Hamilton, 2007; Morlok, Bowey, et al., 2006; Morlok, Kohler, et al., 2006; Morlok et al., 2010). In addition, many studies have noted that microscopic reflectance measurements are affected by crystal orientation in samples. Nonisotropic crystals will exhibit variable thermal infrared spectra depending on grain orientation relative to the incident beam (e.g., Jaret, Johnson, Sims, DiFrancesco, et al., 2018; Martin et al., 2018; Pernet-Fisher et al., 2017).

3. Materials and Methods

3.1. Samples

We used the basalt and basaltic andesite rocks from Johnson et al. (2007), who experimentally shocked samples at 10 to 11 specific pressure levels ranging from ~17 to ~63 GPa. The starting sample for each experimental pressure step was taken from the same rock core. The basalt was from the base of the Grand Falls (AZ) lava flow and contained glass (11%), pyroxene (28%), olivine (4%), and plagioclase (48%) with an average composition of labradorite (~An₅₇). The basaltic andesite was a finer-grained sample from the west side of the SP Flow (AZ) cone, and contained more glass (31%), less pyroxene (18%), some olivine (<1%), and plagioclase (45%) with average composition of andesine (~An₄₈). The Flat Plate Accelerator at the Johnson Space Center was used to conduct the shock experiments through a shock-reverberation process (Gibbons & Ahrens, 1971). Chips recovered from the shocked samples ranged from 2 to 10 mm. The Johnson Space Center sample numbers and experimental shock pressures are listed in Table 1.

3.2. Data Acquisition

Polished thin sections were made from the shocked chip samples. A standard Olympus petrographic microscope was used to obtain cross-polarized and plane-polarized transmitted light images, as shown in Figures 1 and 2 for representative unshocked and shocked samples at shock levels of 0, ~29, and ~57 GPa. Owing to the relatively isotropic nature of the samples when viewed between crossed polarizers, those images were enhanced using a gamma correction ($\gamma = 3$). (The supporting information includes images of samples from all shock pressures.)

Micro-FTIR hyperspectral maps of thin sections were obtained using a liquid nitrogen-cooled HgCdTe (MCT) detector with a Nicolet iN10MX FTIR microscope in the Center for Planetary Exploration at Stony Brook University. Hyperspectral images were acquired between 7,000 and 715 cm⁻¹ (1.4–14.0 μm) at 25 μm/pixel and 8-cm⁻¹ spectral sampling. Observations of gold mirrors were acquired as background measurements prior to each sample, using the same spot size and acquisition times as the sample. Spectra were normalized to 100% maximum reflectance for ease of comparison. Table 1 includes the number of 2-D infrared hyperspectral images made from the thin sections from each sample.

Micro-Raman spectra were acquired of a variety of regions in each sample using the Center for Planetary Exploration (CPEX) WiTec alpha300R confocal imaging system equipped with 532-nm neodymium:

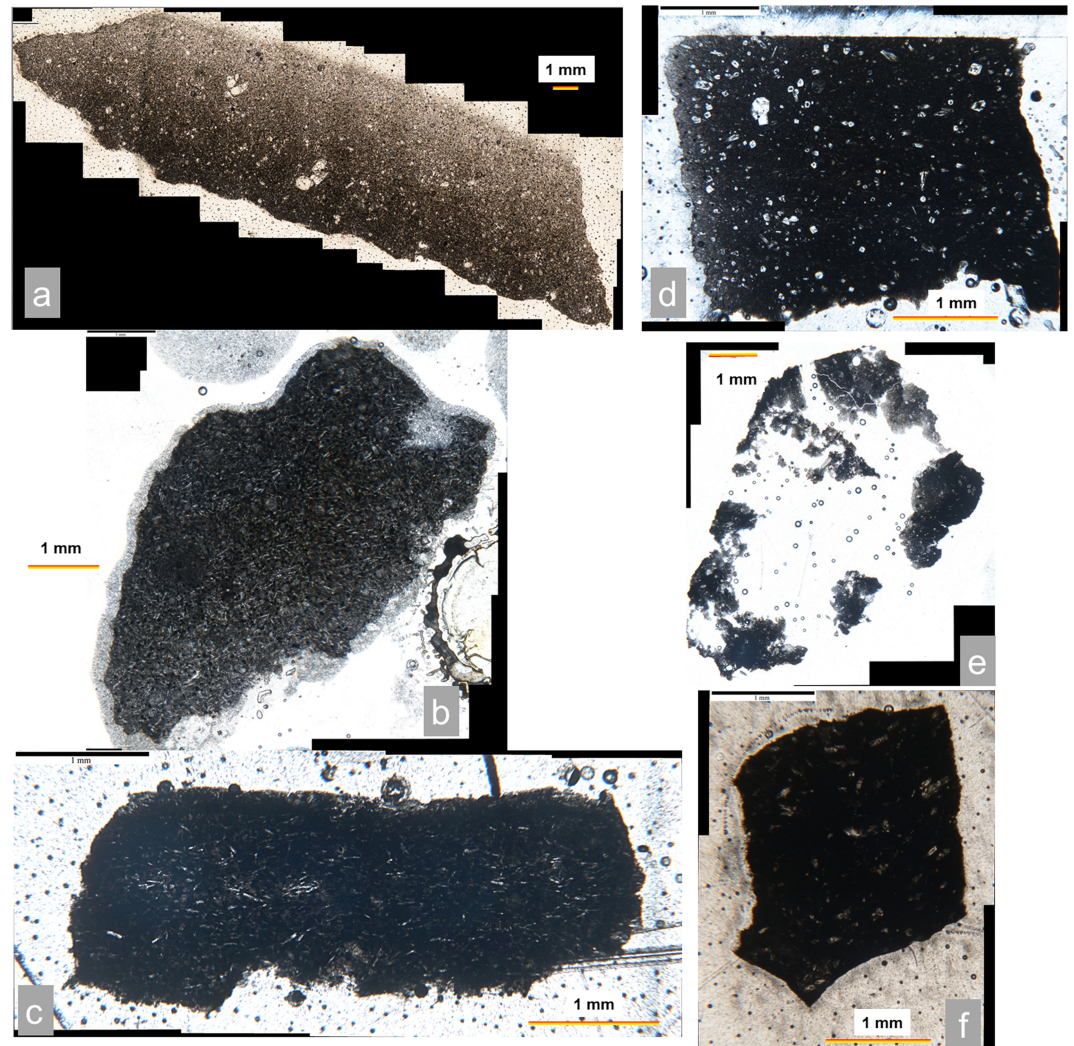


Figure 1. Plane-polarized photomicrographs of (left column) Grand Falls and (right column) SP Flow at different shock pressures: (a) unshocked, (b) 29.0 GPa, (c) 56.8 GPa, (d) unshocked, (e) 28.4 GPa (note much of central sample region is missing and filled with epoxy), and (f) 57.5 GPa. Grand Falls samples (a–c) are larger grained, with distinct plagioclase laths visible, compared to the SP Flow samples (d–f) that show phenocrysts in an otherwise very fine grained groundmass.

yttrium/aluminum/garnet laser with 2.24-mW nominal power at the sample surface, and a 50X (NA = 0.8) objective (resulting in spot size of 763 nm). Each analysis consisted of 240 one-second integrations that were averaged. To alleviate potential uncertainties induced by baseline correction or background subtraction techniques, Raman spectra are provided as raw data with arbitrary intensity units.

3.3. Data Analysis

3.3.1. Thermal Infrared Spectra

The thermal infrared hyperspectral image cubes for each thin section were used to create images to emphasize spectral variability, including false color (red = $1,103\text{ cm}^{-1}$, green = $1,018\text{ cm}^{-1}$, blue = 787 cm^{-1}), $1,103\text{-cm}^{-1}$ “band depth” maps (reflectance band height maps), and $1,103/1,018\text{-cm}^{-1}$ ratio maps (Figures 3 and 4). In combination with the optical thin section images, these maps were used to guide the manual selection of locations from which spectra were extracted from 3×3 -pixel ($75 \times 75\text{ }\mu\text{m}$) areas in the hyperspectral image cubes of representative end-member assemblages. These regions are numbered in Figures 3a–3c and 4a–4c, and are shown in Figure 5 with laboratory spectra for comparison. Supporting information included with this paper contains similar derived data products for all samples listed in Table 1.

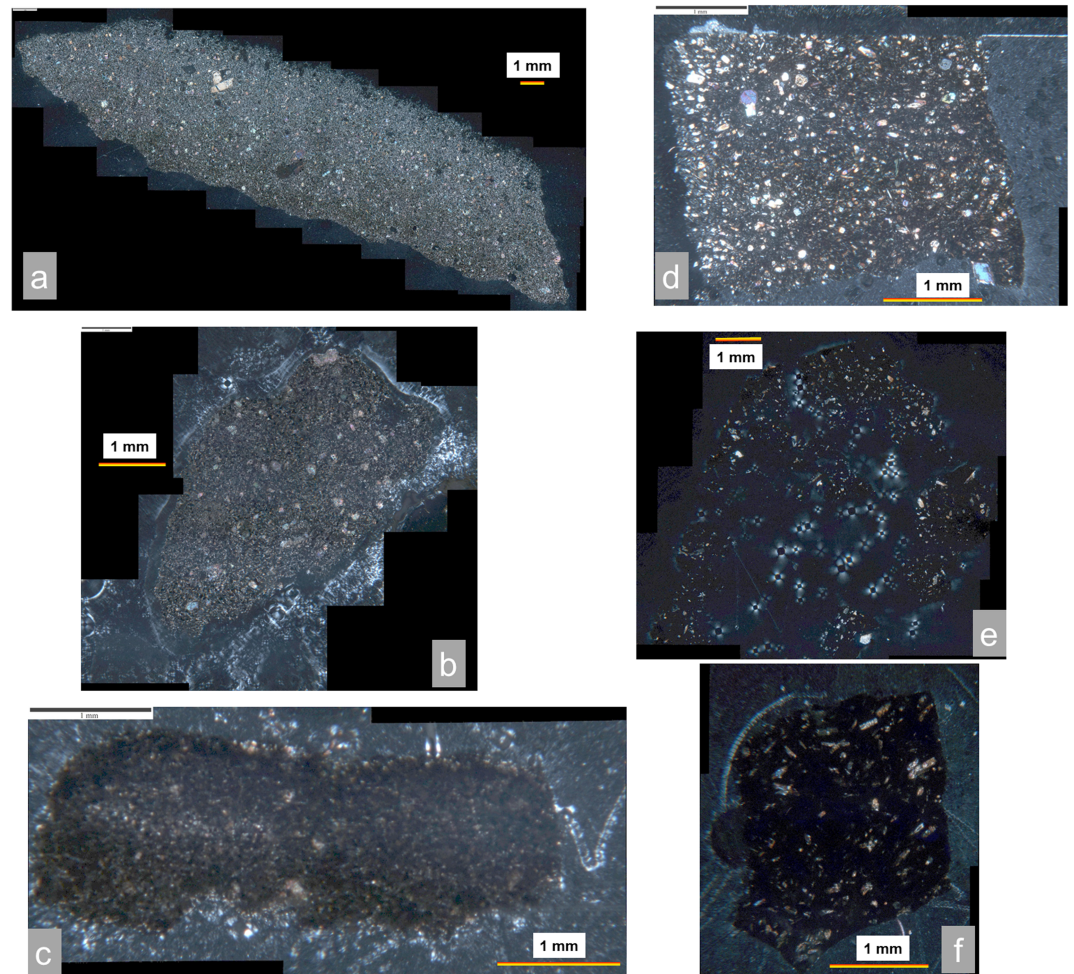


Figure 2. Cross-polarized photomicrographs (contrast stretched with gamma correction = 3) of (left column) Grand Falls and (right column) SP Flow at different shock pressures: (a) unshocked, (b) 29.0 GPa, (c) 56.8 GPa, (d) unshocked, (e) 28.4 GPa (note much of central sample region is missing and filled with epoxy), and (f) 57.5 GPa.

Average spectra were calculated from each thin section hyperspectral image for comparison to bulk emissivity spectra obtained from the original extracted chip samples (Johnson et al., 2007) as shown in Figures 6b and 6e. Also presented are average spectra of plagioclase or maskelynite end-member pixels obtained through the Spectral Angle Mapper (SAM) supervised classification tool within the Environment for Visualizing Images (ENVI) software package. The SAM algorithm determines spectral similarity by comparing the angle between each pixel vector in n -D space and the end-member spectrum vector, where closer matches to the reference spectrum are represented by smaller angles. We selected a region of interest within each hyperspectral image with a typical plagioclase or maskelynite spectrum (usually regions with lime-green colors in the false-color images shown in Figures 3a–3c and 4a–4c) and used a constant maximum angle (0.08 radians) in all SAM calculations. Pixels meeting these criteria were used to create a mask that allowed extraction of average spectra (Figures 6c and 6f). The mask was also used to extract average reflectance band heights at $1,103\text{ cm}^{-1}$ and their standard deviations, as shown in Figure 7 as a function of shock pressure for each thin section's 2-D infrared map (cf. Table 1).

3.3.2. Raman Spectra

Raman spectra were acquired at locations selected in optical mosaics either to provide regions of crystals sufficiently large to encompass the 763-nm spot size, or to represent areas typical of the thin section. Figure 8 shows these locations for the three representative thin sections, and Figures 9 and 10 show the Raman spectra with prominent peaks labeled. These spectra (along with all other samples provided in the supporting information) were analyzed to identify major peaks in each spectrum. Typical peak

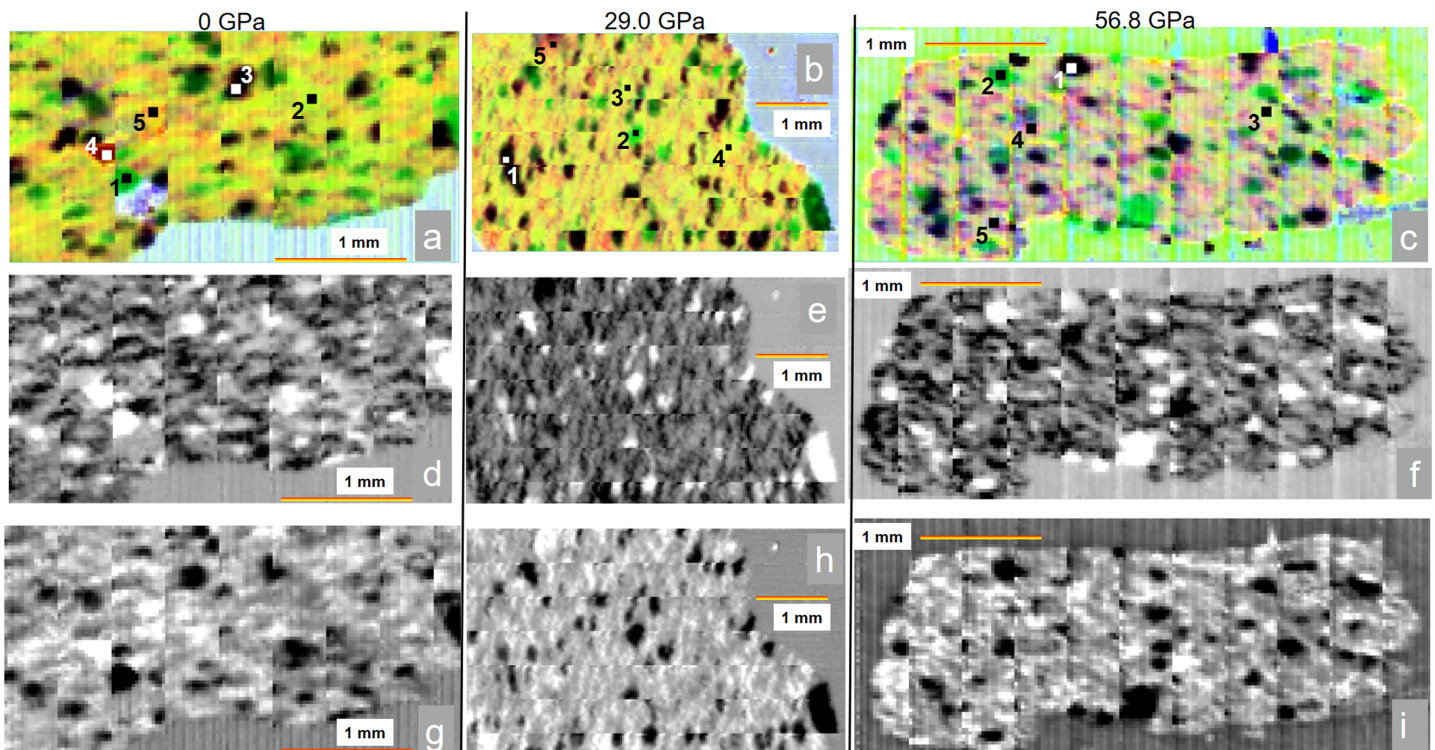


Figure 3. Grand Falls spectral parameter images for (a–c) false color (using red = $1,103\text{ cm}^{-1}$, green = $1,018\text{ cm}^{-1}$, blue = 787 cm^{-1}), (d–f) $1,103\text{-cm}^{-1}$ reflectance band height, and (g–i) $1,103/1,018\text{ cm}^{-1}$ ratio at (left column) 0 GPa, (middle column) 29.0 GPa, and (right column) 56.8 GPa. Numbered points in false-color images designate approximate areas from which spectra were extracted (Figure 5).

positions included those associated with plagioclase near 480 and 510 cm^{-1} related to the stretching motion of the SiO_4 or AlO_4 tetrahedra (Freeman et al., 2008; Mernagh, 1991). Comparison to laboratory data of standard minerals (Figure 11) demonstrates other Raman peaks associated with olivine doublet Si–O symmetric stretching modes ($824, 855\text{ cm}^{-1}$) or pyroxene Si–O–Si stretch (670 cm^{-1}) and Si–O bridging stretch modes ($1,015\text{ cm}^{-1}$; cf. Wang et al., 1995, 2001, 2015). These were not tracked as a function of pressure owing to their greater resistance to shock at the pressures examined here (e.g., Farrell-Turner et al., 2005; Harriss & Burchell, 2016; Johnson et al., 2002; Zhang et al., 2018). The broad humps near $1,000\text{ cm}^{-1}$ may also vary with composition (Al–O to Si–O ratios) in plagioclase glass or maskelynite (e.g., Fritz et al., 2019).

For reference, the Raman spectra from experimentally shocked andesine- and bytownite-rich rocks from Jaret, Johnson, Sims, DiFrancesco, et al. (2018) are shown in Figure 12 (which bracket the plagioclase compositions of the basalts studied here). These exemplify the loss of Raman peaks with increasing pressure for the three representative shock pressures presented here. The peak intensities for the dominant bands decreased substantially with pressure as the plagioclase became more disordered, where the peak intensity ratios of $\sim 480/\sim 505\text{ cm}^{-1}$ exhibited a weak positive linear correlation with increasing pressure. Figure 13 shows similar peak intensity ratios for those plagioclase pixels categorized using the SAM technique, which also show a weak positive linear correlation, as discussed further below.

4. Results

4.1. Petrography

Unshocked Grand Falls samples showed typical fabrics of basalts, containing plagioclase, clinopyroxene, and minor olivine. Plagioclase laths were fine-grained, approximately $100 \times 20\text{ }\mu\text{m}$. Olivine and pyroxene were subhedral to euhedral and approximately $100\text{ }\mu\text{m}$. Shock effects in the Grand Falls samples were limited to only within plagioclase. Plagioclase in the shocked samples showed slight decreases in birefringence

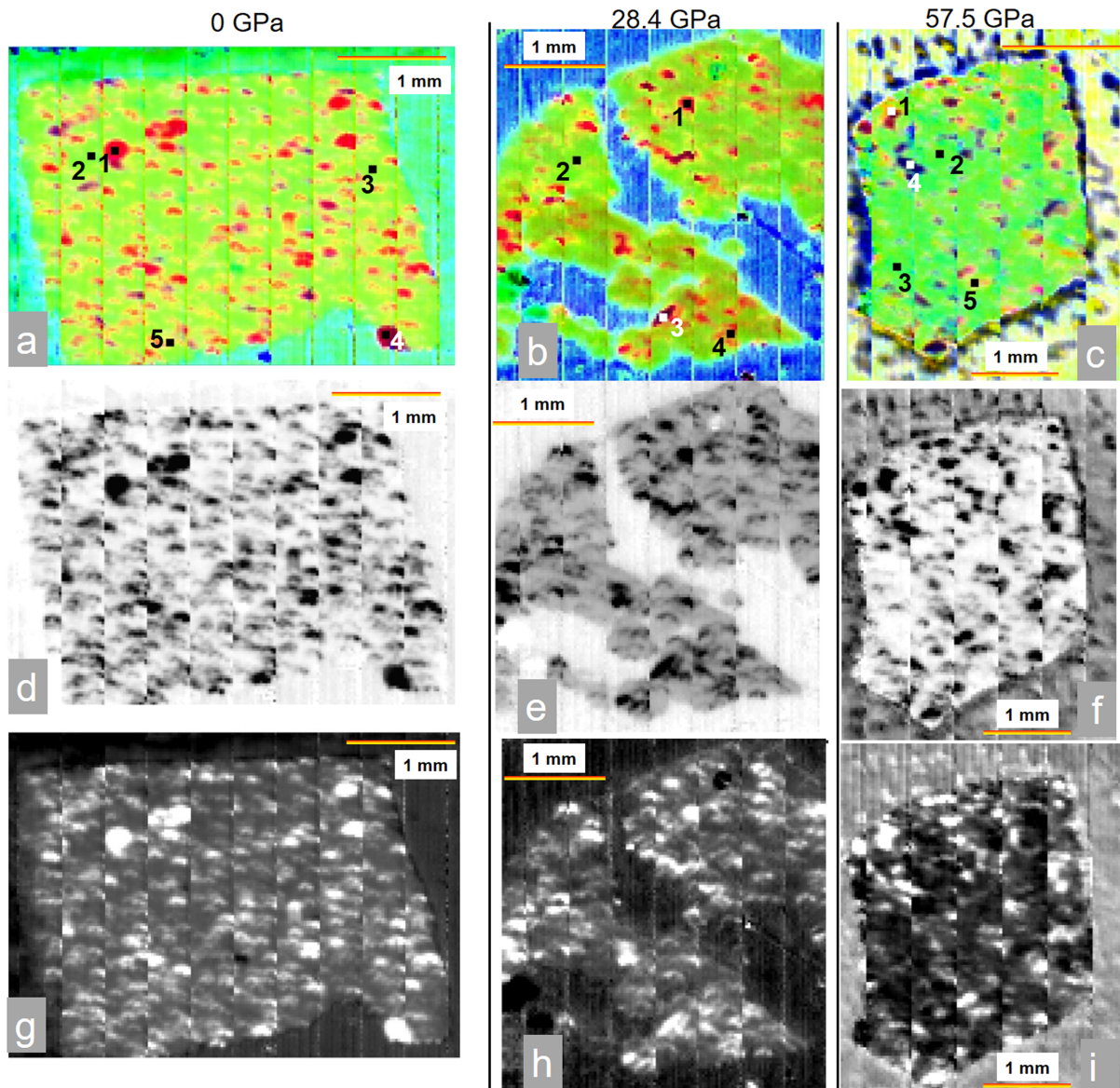


Figure 4. SP Flow spectral parameter images for (a–c) (false color, using red = $1,103\text{ cm}^{-1}$, green = $1,018\text{ cm}^{-1}$, blue = 787 cm^{-1}), (d–f) $1,103\text{-cm}^{-1}$ reflectance band height, and (g–i) $1,103/1,018\text{-cm}^{-1}$ ratio at (left column) 0 GPa, (middle column) 28.4 GPa, and (right column) 57.5 GPa. Numbered points in false-color images designate approximate areas from which spectra were extracted (Figure 5).

between 17.2 and 26.7 GPa, but did not show mosaicism or undulatory extinction. In all samples above 26.7 GPa all the plagioclase grains were uniformly isotropic, yet retained grain boundaries. No flow textures were observed within plagioclase grains nor was there evidence for polymineralic melt generation. Olivine and pyroxene remained birefringent throughout all pressure steps, and did not show any textural evidence of shock deformation.

SP Flow samples exhibited smaller plagioclase grains than Grand Falls ($\sim 50 \times \sim 10\ \mu\text{m}$), whereas pyroxene phenocrysts were up to $50\text{--}60\ \mu\text{m}$. Additionally, SP contained up to 30% glass. In the shocked samples plagioclase appeared isotropic at 17.2 GPa and in all samples of higher pressure. Similar to Grand Falls, the plagioclase retained its grain boundaries and showed no evidence of internal melting or vesiculation. Pyroxenes and olivine remained birefringent throughout all pressure steps, and lacked cracking, fracturing, or other textural effects of shock deformation.

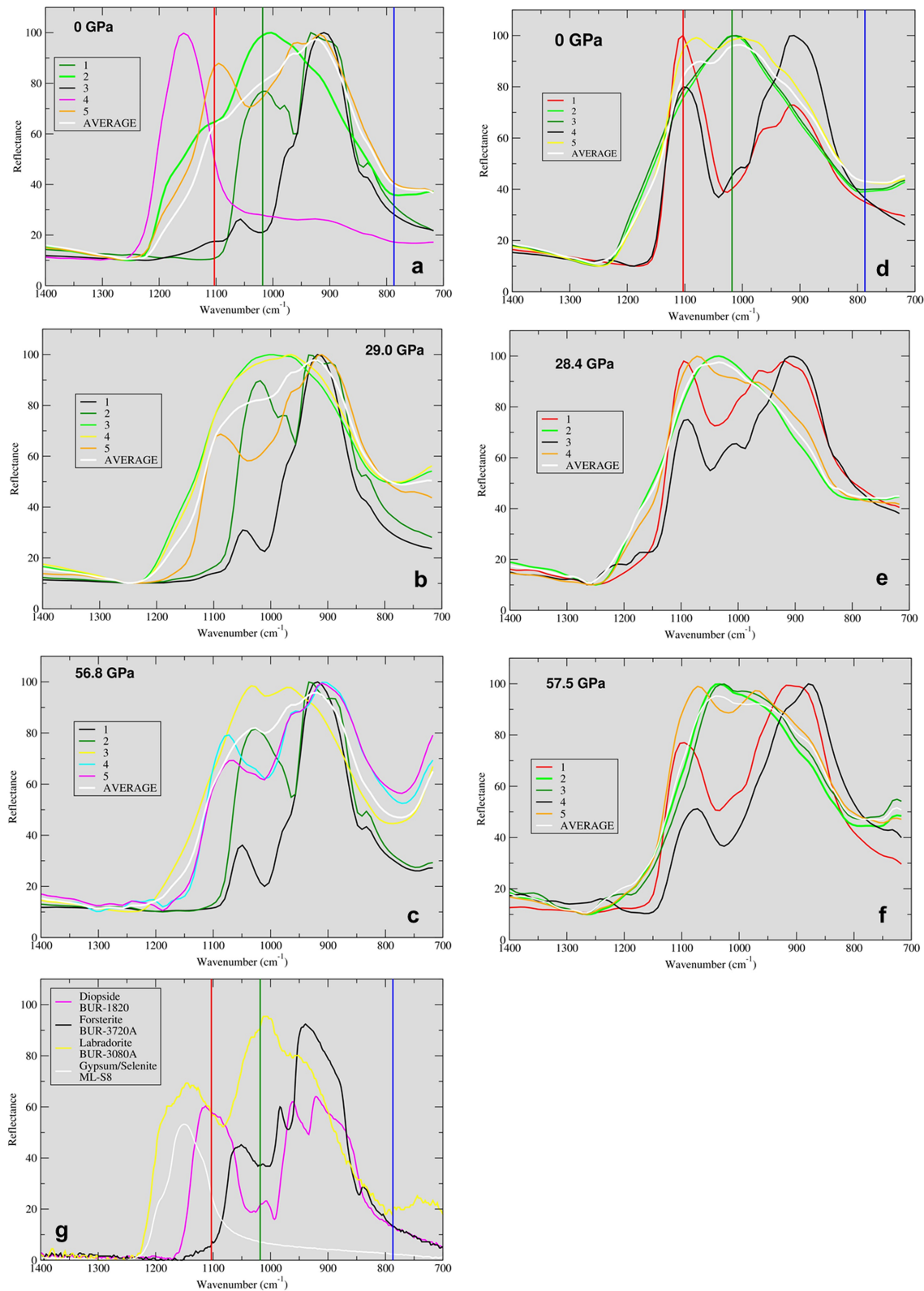


Figure 5. Thermal infrared spectra extracted from hyperspectral images of (a–c) Grand Falls and (d–f) SP Flow at pressures shown. Numbered locations correspond to those shown in Figures 3 and 4. Each spectrum represents a 3×3 -pixel ($75 \times 75 \mu\text{m}$) region. Average spectrum for entire sample shown in white (cf. Figures 6a and 6d). Laboratory spectra of example minerals from Christensen et al. (2000) are shown in (g), converted to reflectance for ease of comparison. Vertical lines represent bands used in false-color images shown in Figures 3 and 4 (red = $1,103 \text{ cm}^{-1}$, green = $1,018 \text{ cm}^{-1}$, blue = 787 cm^{-1}).

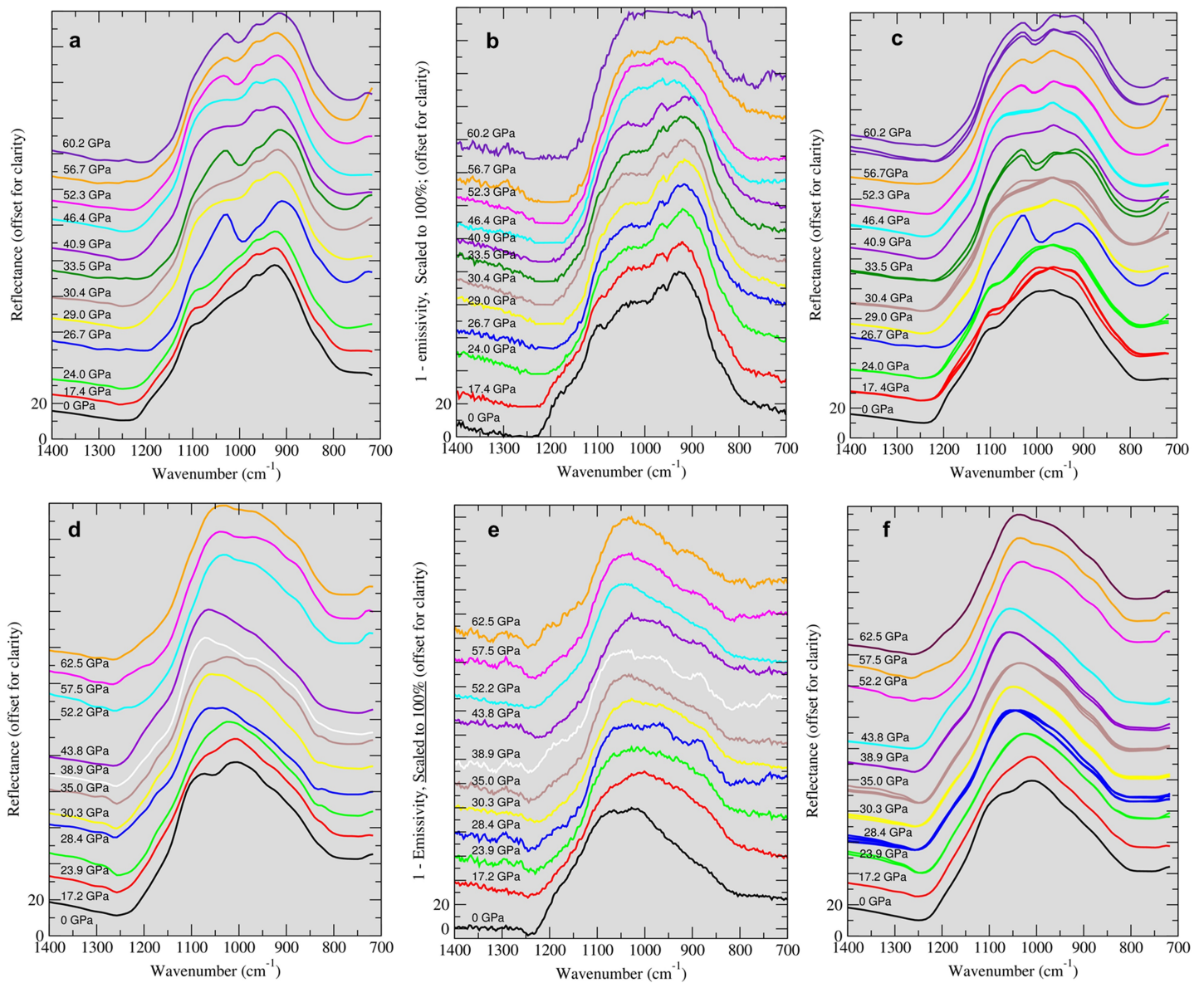


Figure 6. Average thermal infrared spectra extracted from hyperspectral images of entire thin section for (a) Grand Falls and (d) SP Flow samples, offset and labeled with peak shock pressure. For comparison, emissivity spectra of chip samples from Johnson et al. (2007) (converted to reflectance and scaled to 100%) are shown for (b) Grand Falls and (e) SP Flow samples. Also shown are collections of average plagioclase/maskelynite spectra from (c) Grand Falls and (f) SP Flow hyperspectral maps (see text). Note the absorption near $1,000\text{ cm}^{-1}$ in the higher pressure Grand Falls samples (a–c) that is discussed in section 5.2.

4.2. Infrared Spectroscopy

The spectra extracted from the 2-D hyperspectral images (Figures 3 and 4) verify that the Grand Falls unshocked sample is dominated by plagioclase, olivine, and pyroxene, with minor minerals such as gypsum. The SP Flow unshocked sample contains similar major minerals, but a less well defined plagioclase spectrum that is likely a consequence of its finer grain size and higher primary glass content compared to the Grand Falls sample. Both samples are sufficiently fine-grained that the $75 \times 75\text{-}\mu\text{m}$ regions of interest from which spectra were extracted often comprised multiple minerals, including the presence of plagioclase microlites and/or crystalline domains in the mesostasis (Johnson et al., 2007). For example, spectrum 3 in Figure 5a exhibited spectral features consistent with both olivine and plagioclase, although variations in crystal orientations could shift peak locations and increase uncertainty in some specific mineral identifications (cf. Jaret, Johnson, Sims, DiFrancesco, et al., 2018; Martin et al., 2018; Pernet-Fisher et al., 2017, and

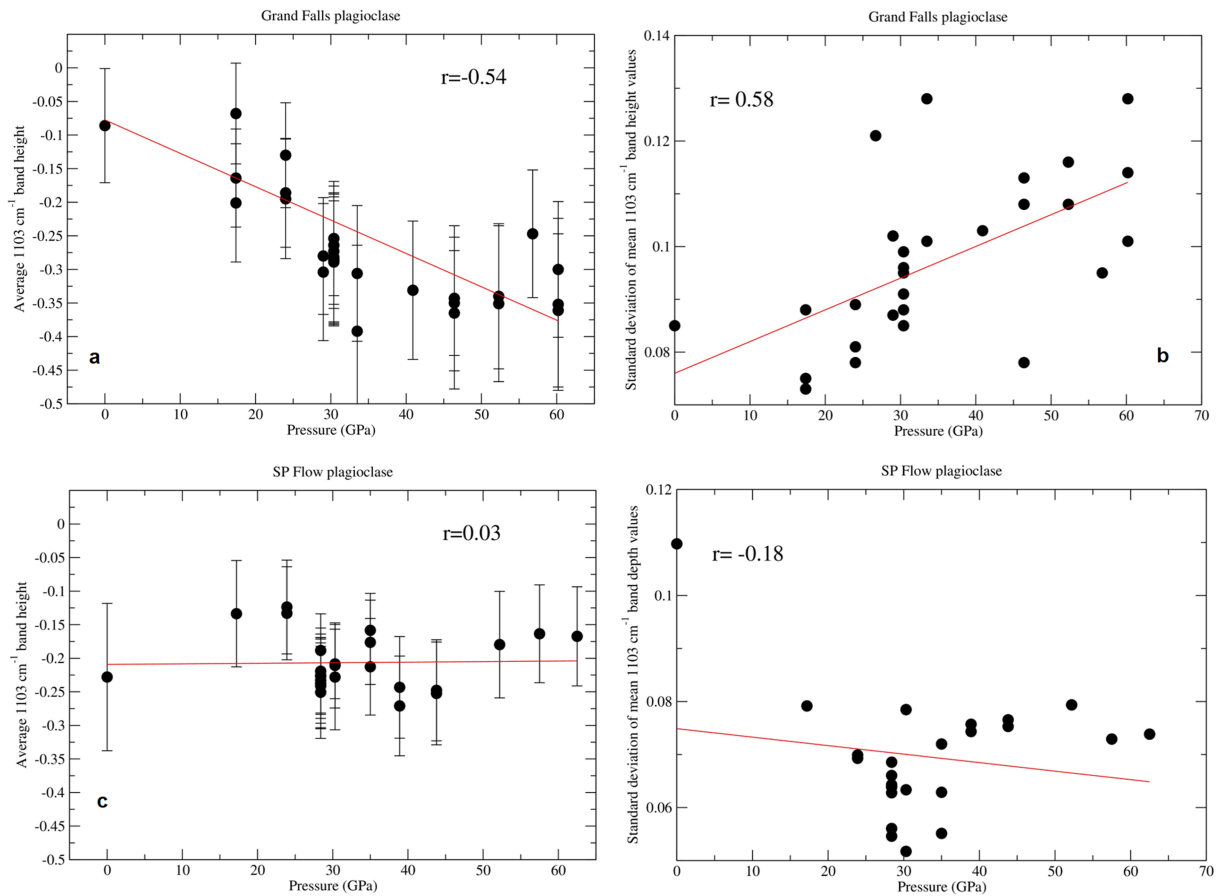


Figure 7. Average $1,103\text{-cm}^{-1}$ reflectance band heights computed from average plagioclase spectra (Figure 6) for (a) Grand Falls and (c) SP Flow samples as a function of shock pressure, alongside (b and d) standard deviations of those averages. Each point corresponds to an individual 2-D infrared map (Table 1). Grand Falls samples exhibit moderate negative correlation between reflectance band heights and pressure, reaching a minimum at about -0.35 for samples above ~ 30 GPa. Grand Falls standard deviations exhibited a moderate positive correlation with pressure. SP Flow samples exhibit no correlations with pressure.

references therein). At higher shock pressures (Figures 5b/5e and 5c/5f) the plagioclase spectra lost their prominent spectral features and exhibited a broad peak centered near $950\text{--}1,000\text{ cm}^{-1}$ in the Grand Falls samples and near $1,000\text{--}1,060\text{ cm}^{-1}$ in the SP Flow samples. This difference in peak positions is consistent with the more calcic nature of the plagioclase in Grand Falls samples (cf. Jaret, Johnson, Sims, DiFrancesco, et al., 2018; Johnson et al., 2002, 2007).

Some shocked Grand Falls samples also exhibited an inconsistent and unusual spectral band centered near $1,000\text{ cm}^{-1}$. This feature appeared in several of the average reflectance spectra from higher-pressure samples (Figure 6a; 26.7, 33.5, 52.3, 56.7, and 60.2 GPa). It also occurred in some of the macroscale emissivity spectra from Johnson et al. (2007) (Figure 6b; 24.0–40.9 GPa). The plagioclase and/or maskelynite average spectra extracted using the SAM algorithm (Figure 6c) also exhibit the $1,000\text{-cm}^{-1}$ band, suggesting that plagioclase and/or maskelynite are responsible for this band. Comparisons to laboratory mineral spectra suggest that this spectral feature derives from contributions of olivine and pyroxene to the maskelynite spectrum (cf. Figure 5g) at spatial scales below the region of interest size ($75 \times 75\ \mu\text{m}$). The prevalence of such fine-grained combinations depends on the nature of shock propagation through variable distributions of crystalline, glass, and mesostasis materials among the unshocked samples. The suppression of this band in some of the macroscale spectra in Figures 6b and 6e (Johnson et al., 2007) may result from a combination of averaging over a greater sample area ($\sim 1\text{ cm}$) that includes more types of minerals and glasses than observed at $75 \times 75\text{-}\mu\text{m}$ scales, and/or the influence of more randomized crystal orientations, both of which would serve to subdue the $1,000\text{-cm}^{-1}$ band.

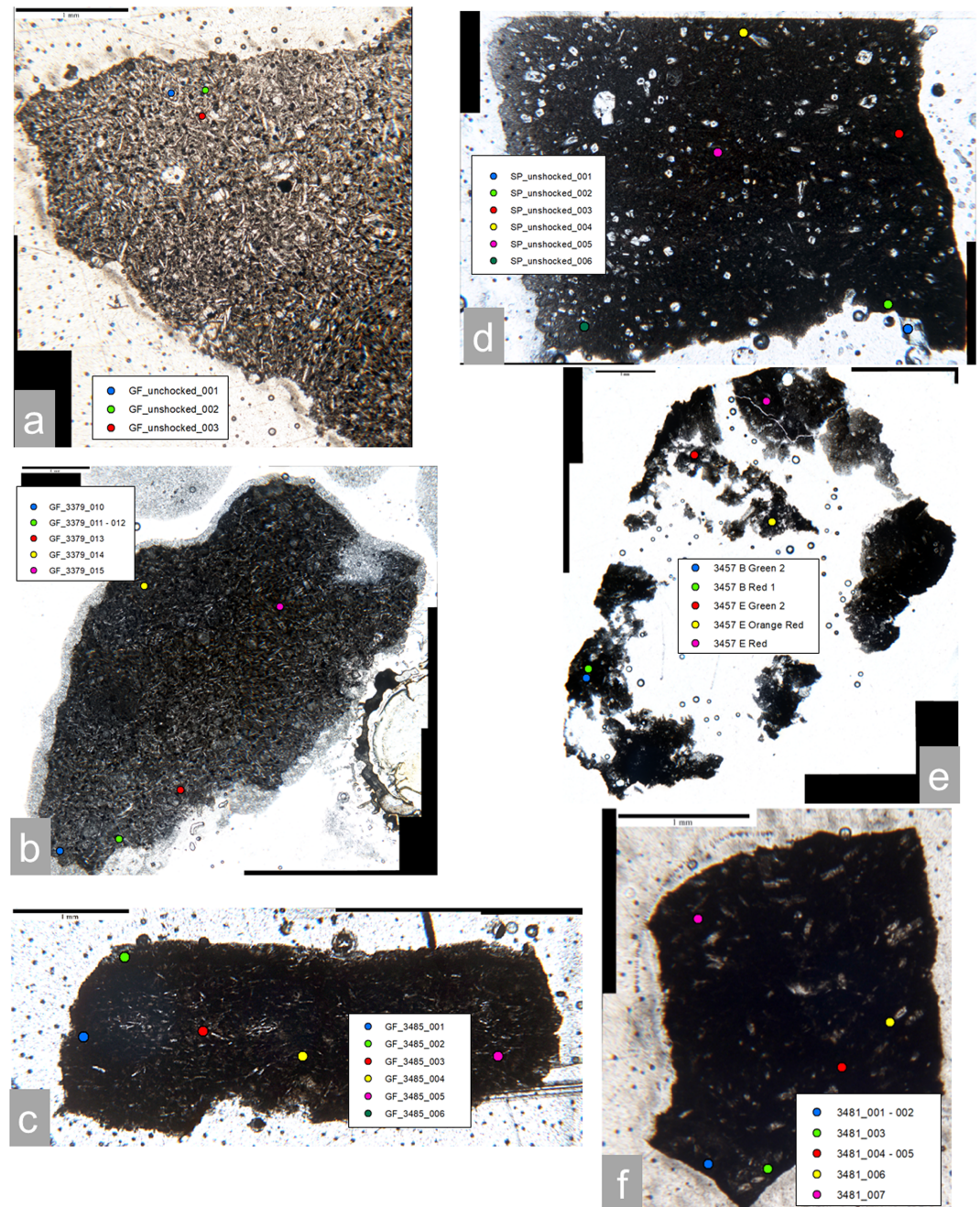


Figure 8. Locations of Raman spectra (shown in Figures 9 and 10) shown on plane-polarized photomicrographs for (left column) Grand Falls (GF) and (right column) SP Flow (SP) at different shock pressures: (a) unshocked, (b) 29.0 GPa, (c) 56.8 GPa, (d) unshocked, (e) 28.4 GPa, and (f) 57.5 GPa. Spectral locations with two sample numbers correspond to locations within the size of the colored circle.

Using microscopic hyperspectral images of shocked plagioclase, Jaret, Johnson, Sims, DiFrancesco, et al. (2018) demonstrated that the depths (or peaks in reflectance spectra) of the 950–1,150- cm^{-1} reststrahlen bands exhibited variable positive linear correlations with pressure, depending on the plagioclase composition or band of interest. They also demonstrated that the standard deviation of those averages often exhibited a negative correlation with pressure, suggestive of increasing homogeneity of the samples at the scale of observation ($75 \times 75 \mu\text{m}$). Figure 7 shows the average 1,103- cm^{-1} reflectance band heights and standard deviations for both basaltic samples. The Grand Falls sample exhibited a decrease in band height with

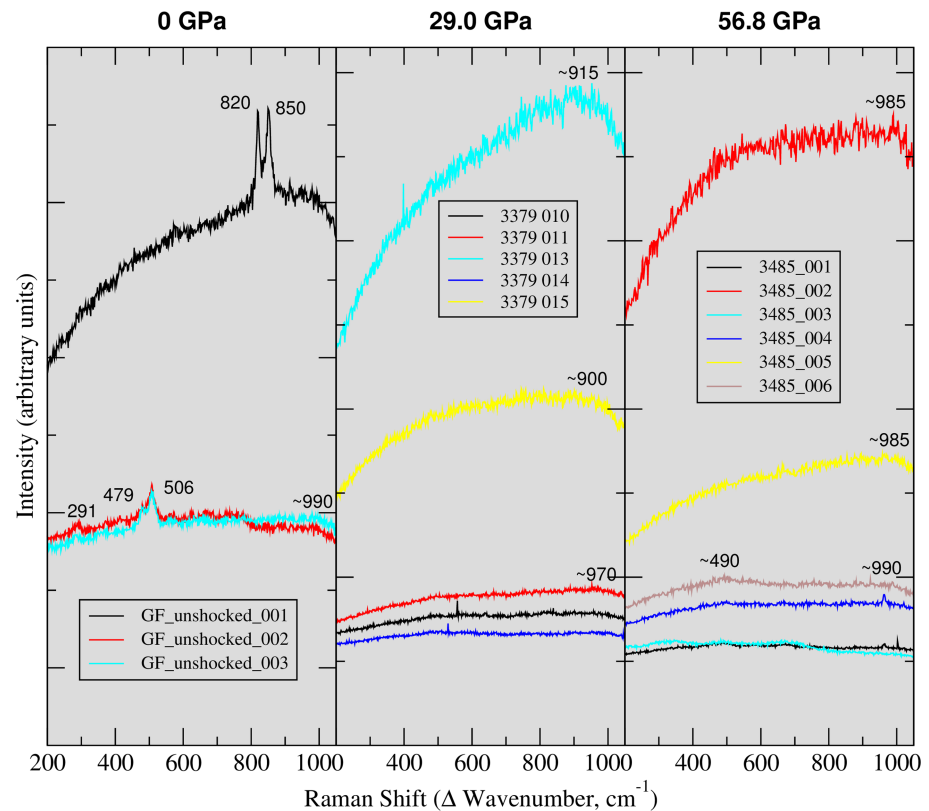


Figure 9. Example Raman spectra extracted from Grand Falls samples (cf. Figure 8 for locations), with approximate spectral peak positions labeled. Compare to Figure 11 for typical peaks associated with representative minerals. The spectra were not baseline corrected or background subtracted and the intensities are given in arbitrary units.

pressure until 33.5 GPa, at which point a value of about -0.35 was maintained. The standard deviations increased moderately with pressure, suggesting that the samples became more heterogeneous at the $75\text{-}\mu\text{m}$ scale, as discussed below. Conversely, the SP Flow exhibited no correlations with either average band height or standard deviations (Figures 7c and 7d).

4.3. Raman Spectroscopy

Raman spectra of selected locations in the Grand Falls and SP Flow samples show peaks associated with plagioclase, pyroxene, and olivine (Figures 9 and 10). Some spectra exhibited peaks representative of multiple minerals even within the 763-nm spot size (e.g., Figures 10 (spectra 003 and 006) and S3g (spectrum 004)), owing to the fine grain size of the samples. Although olivine and pyroxene peaks remain present through all pressures, plagioclase peaks were lost at relatively low shock pressures and transitioned to weak, broad peaks after $\sim 24\text{--}29$ GPa. Along with the plots in the supporting information, Figure 13 demonstrates this by plotting the intensity ratios of the two main plagioclase peaks near 480 and 510 cm^{-1} as a function of pressure. A positive correlation is shown, but it is also apparent that the ratio values leveled to near 1.0 after pressures of $\sim 24\text{--}29$ GPa in both samples. These values are slightly lower than the pressures at which plagioclase Raman spectral peaks were lost in experimentally shocked andesine and bytownite samples from Jaret, Johnson, Sims, DiFrancesco, et al. (2018) (Figure 12). This may result from the primary glass in the basaltic samples studied here, which tends to exhibit one broad band near this spectral region rather than two separate peaks (e.g., Fritz et al., 2019; Gucsik et al., 2004; Prinsloo et al., 2011). The lower pressures for amorphization may be due to either the smaller grain size of the plagioclase compared to the nearly monomineralic plagioclase rocks used in previous shock experiments (Johnson, 2012; Johnson et al., 2002, 2003). Alternatively, this could be due to impedance with the higher-density pyroxenes, which would tend to generate slightly higher particle velocities (and average shock levels) compared to the more monomineralic plagioclase samples.

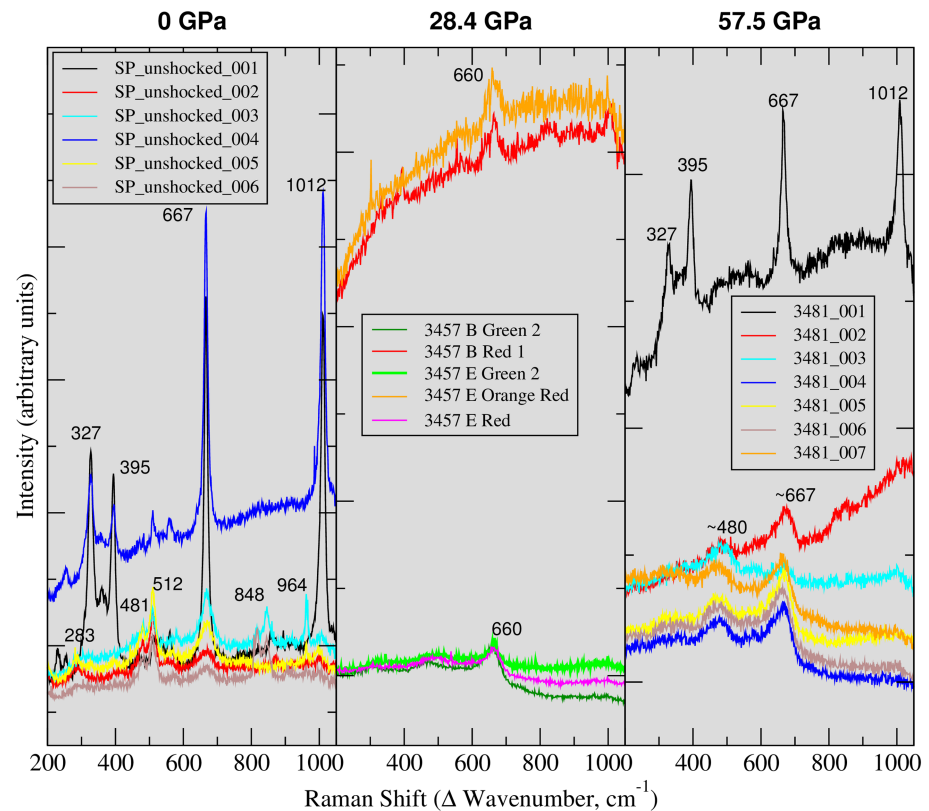


Figure 10. Example Raman spectra extracted from SP Flow samples (cf. Figure 8 for locations), with approximate spectral peak positions labeled. Compare to Figure 11 for typical peaks associated with representative minerals. The spectra were not baseline corrected or background subtracted and the intensities are given in arbitrary units.

5. Discussion

Jaret, Johnson, Sims, DiFrancesco, et al. (2018) noted that thermal infrared and Raman spectra of experimentally shocked plagioclase exhibited heterogeneity at scales $<75 \mu\text{m}$ such that amorphous materials would be in direct contact with more crystalline grains, as is often observed in natural impact samples. They suggested that this could result from shockwave heterogeneities either within the shock wave itself, from refractions and associated impedance mismatches among adjacent grains, or from variations in crystal orientation. In their analysis of the Northwest Africa 8159 meteorite, Herd et al. (2017) noted a relationship between crystalline plagioclase and shock-amorphized phases of plagioclase (An_{50-62}) directly associated with shock veins. They presented Raman spectra of plagioclase in the host rock with peaks at 480 and 509 cm^{-1} , and plagioclase glass with a broad hump near 509 cm^{-1} . This is similar to the broad peaks between 487 and 498 cm^{-1} that Jaret, Johnson, Sims, DiFrancesco, et al. (2018) identified in micro-Raman spectra of experimentally shocked andesine and bytownite, respectively, beginning at shock pressures near $28\text{--}29 \text{ GPa}$.

The types of heterogeneities noted by Jaret, Johnson, Sims, DiFrancesco, et al. (2018) were observed in the basaltic samples studied here, likely resulting from a combination of multiple species and sizes of mineral grains, interstitial primary glass, and mesostasis within the original, unshocked rock samples. Plagioclase in the Grand Falls and SP Flow samples were noted from petrographic analyses here to become amorphous at different pressures. This could be explained by the finer sizes of the SP Flow plagioclase grains, which were more easily converted to glass because of the shorter length scales of dislocations, as well as the slightly different plagioclase composition between the Grand Falls ($\sim\text{An}_{57}$) and SP Flow ($\sim\text{An}_{48}$) plagioclase. Additionally, the larger and higher-density pyroxene grains in the SP Flow sample could generate slightly higher local shock conditions because of impedance mismatching with the plagioclase.

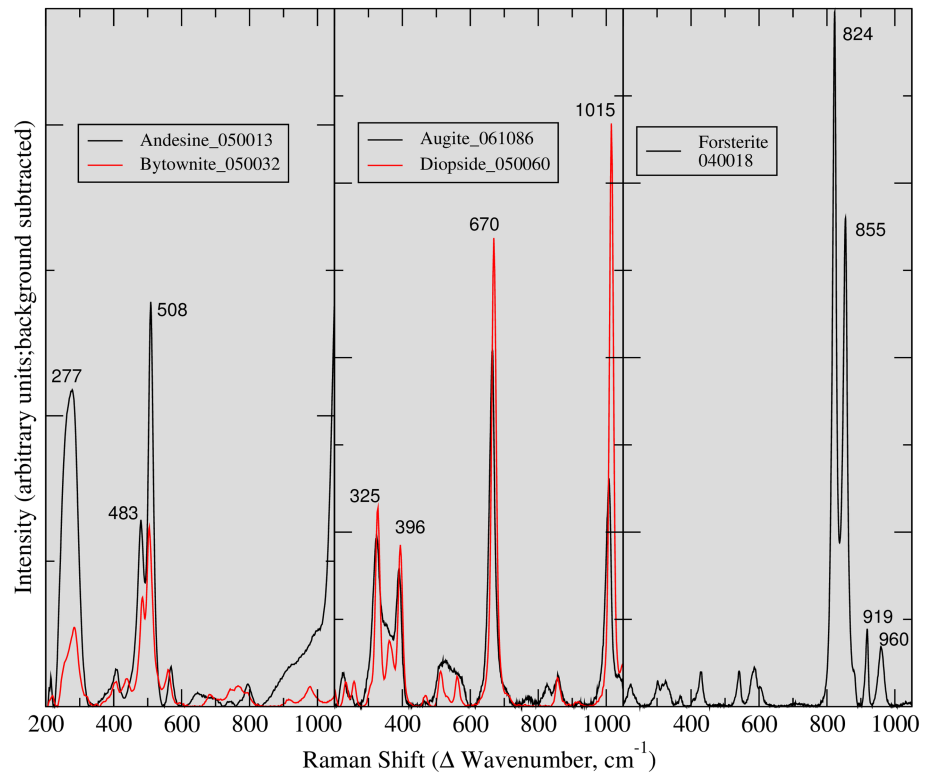


Figure 11. Raman spectra (background-subtracted) of representative minerals from the RRUFF database (<http://rruff.info/>), with relevant peak positions labeled.

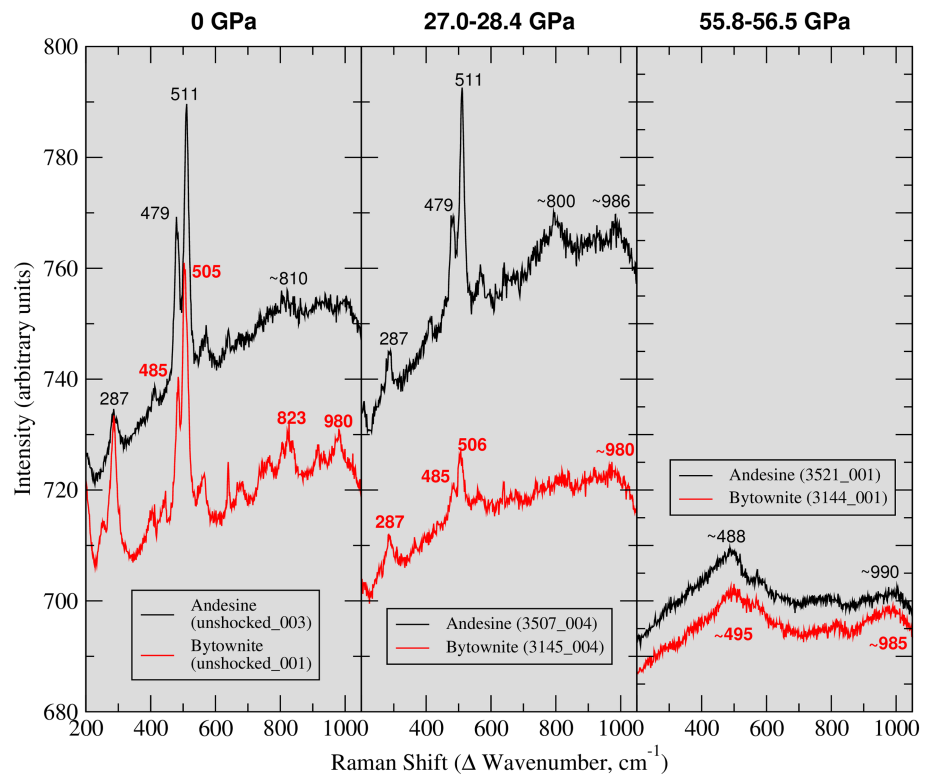


Figure 12. Example Raman spectra of unshocked and shocked andesine and bytownite from Jaret, Johnson, Sims, DiFrancesco, et al. (2018), with approximate spectral peak positions labeled.

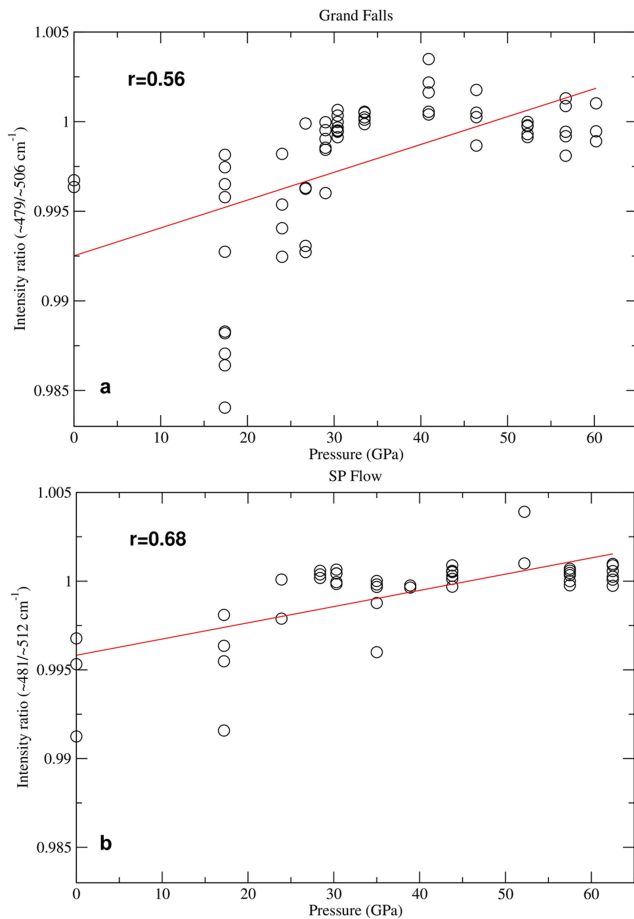


Figure 13. Peak intensity ratios of dominant peaks in Raman spectra of plagioclase-bearing locations in (a) Grand Falls and (b) SP Flow samples as a function of shock pressure, with linear correlations shown.

samples. Also, the effect was less pronounced for the SP Flow samples, likely another indication that the greater amount of primary glass played a key role. Nonetheless, the ~25–30-GPa pressure range was again consistent with the amorphization onset pressure of andesine and increasing presence of maskelynite at higher pressures.

6. Conclusions

Petrographic, micro-Raman, and micro-FTIR infrared spectral analyses of experimentally shocked basalt and basaltic andesite samples indicated that progressive amorphization of plagioclase with increasing pressure (up to ~63 GPa) resulted in detectable spectral variations that mimic those of the experimentally shocked, plagioclase-dominated rocks analyzed in earlier studies (Jaret, Johnson, Sims, DiFrancesco, et al., 2018; Johnson, 2012; Johnson et al., 2002). However, variations in starting sample composition and/or shock propagation through the minerals and mesostasis within these rocks resulted in variable distribution of shock effects within the samples, which was manifested in their high-resolution infrared and Raman spectra. In particular, the presence of primary glass within the starting materials subdued the apparent pressure effects because of the spectral similarity between the glasses and maskelynite. This resulted in some ambiguity in distinguishing between amorphization caused by shock effects and that associated with initial glass contents, particularly for the more hypocrystalline SP Flow basaltic andesite (~30% glass) compared to the Grand Falls basalt (~10% glass). Nonetheless, infrared reflectance band peaks and Raman peak intensity ratios associated with plagioclase weakened with increasing pressure at slightly lower to comparable shock pressures as those observed for plagioclase-rich rocks by Jaret, Johnson, Sims, DiFrancesco, et al. (2018). As such, the relative contribution of plagioclase to overall knowledge of the

Despite the observed heterogeneities, the average plagioclase thermal infrared spectra extracted from the 2-D hyperspectral images for the Grand Falls samples exhibited a moderate negative correlation between the $1,103\text{-cm}^{-1}$ reflectance band heights and shock pressure until ~30 GPa (Figure 7a). This is consistent with the andesine amorphization onset pressure determined by Jaret, Johnson, Sims, DiFrancesco, et al. (2018) of 28.4–29.4 GPa. However, unlike the moderate negative correlation of the standard deviation of similar band depths with pressure for the Jaret, Johnson, Sims, DiFrancesco, et al. (2018) plagioclase, the Grand Falls samples' band depth standard deviations exhibited a positive correlation (Figure 7b). The implication is that the plagioclase-like spectra became more heterogeneous with increasing pressure. This is consistent with the physical mixing of additional materials within the $75 \times 75\text{-}\mu\text{m}$ region sampled by the spectra. Such mixing could result from increased presence of the olivine and pyroxene grains incorporated with deformed and fractured plagioclase grains at higher pressures. This could help explain the $\sim 1,000\text{-cm}^{-1}$ absorption band observed in several of the more highly shocked Grand Falls samples (Figures 6a–6c), although variations in olivine or pyroxene grain abundance within the original sample splits and/or residual effects caused by crystal orientation variations cannot be ruled out. For comparison, the SP Flow samples' plagioclase-like spectra exhibited no band depth or standard deviation correlations with pressure, and none exhibited the $\sim 1,000\text{-cm}^{-1}$ band (Figures 6d–6f, 7c, and 7d). The most straightforward explanation is that the 3 times greater primary glass content in the unshocked SP Flow samples resulted in spectra that were sufficiently similar to maskelynite spectra so as to result in little apparent variation with pressure.

The plagioclase-bearing Raman spectra for both Grand Falls and SP Flow samples exhibited a moderate positive correlation between peak intensity ratios and shock pressure (Figure 13). In both samples constant ratio values near 1.0 were reached after pressures of ~25–30 GPa, although the scatter among the Raman points demonstrated the variability in the

shock state still holds some promise even in complicated, multicomponent basaltic rocks, albeit depending on their primary glass content. It is noteworthy that attempts to use the shocked plagioclase infrared spectra in linear unmixing models of Thermal Emission Spectrometer orbital spectra of Mars (Johnson et al., 2006; Rogers, 2011; Glotch & Rogers, 2013) and Miniature Thermal Emission Spectrometer spectra from the Mars Exploration Rovers (Ruff et al., 2006; Rogers & Aharonson, 2008) may have resulted in null detections of highly shocked plagioclase in part owing to the difficulty in distinguishing between spectra of primary glass and maskelynite.

Future work would benefit from Raman 2-D mapping efforts (e.g., Foucher et al., 2017; Wang et al., 2015) such as the preliminary data acquired on the 17-GPa Grand Falls sample by Jaret, Johnson, Sims, and Glotch (2018), and/or from visible/near-infrared microimaging (e.g., Manzari et al., 2019). Raman mapping would enable a more spatially comprehensive view of spectral variations at submicron scales, which could provide better insight regarding the influence of grain boundaries and mineralogical variations on shock propagation in fine-grained basaltic samples. Application of these techniques to terrestrial impact samples (e.g., Glotch & Ferrari, 2011; Glotch et al., 2011; Jaret et al., 2013) would also help refine the nature and magnitude of shock propagation effects of naturally shocked samples, whose shock durations are about 10^3 times longer than those associated with laboratory shock experiments. Indeed, many authors have noted that the types of shock experiments used to create these samples encompass different temperatures and/or strain rates than those associated with natural impacts (e.g., Hörz & Cintala, 1997; Jaret, Johnson, Sims, DiFrancesco, et al., 2018; Sharp & DeCarli, 2006). Nonetheless, it is uncertain whether naturally shocked samples would become amorphous at the same pressure values as those generated in the laboratory experiments (cf. Fritz et al., 2019; Sharp et al., 2019; Sharp & DeCarli, 2006).

It is apparent from this work that a priori knowledge of primary glass contents may be necessary in order to fully recognize and/or quantify shock states in basaltic samples when analyzing in situ materials with infrared or Raman methods on planetary surfaces. Variations in spectral features potentially related to shock effects that are observable on the <1-mm scale could reflect mixing of shocked and unshocked materials, particularly if they are associated with the types of veins analyzed in Martian meteorites (e.g., Herd et al., 2017; Sharp et al., 2019). More precise distinctions between impact melts and primary igneous glass may eventually benefit from petrographic analyses of crystal size distributions of the type proposed by Neal et al. (2015), detailed laboratory Raman analyses of returned samples (Fritz et al., 2019), and/or nanofield infrared measurements at submicron scales (Dominguez et al., 2014; Glotch et al., 2019; Kebukawa et al., 2019).

Acknowledgments

This work was supported by Planetary Geology and Geophysics grant NNX14AN33G (J.R.J., P.I.) and the RIS²E node of NASA's Solar System Exploration Research Virtual Institute (SSERVI; T.D.G., P.I.). Data supporting the conclusions can be obtained in the tables and supporting information, and spectra and images can be found on the American Museum of Natural History Library archive (<https://dx.doi.org/10.5531/sd.edu.1>). All data also will be archived in the NASA Planetary Data System (PDS) after publication of this manuscript, as part of the existing archive already containing the plagioclase data from Jaret, Johnson, Sims, DiFrancesco, et al. (2018): https://pds-geosciences.wustl.edu/missions/labdata/shocked_feldspars.htm. The authors thank J. Fritz and A. Pickersgill for their helpful reviews, which substantially improved the paper.

References

- Ahrens, T. J., Petersen, C. F., & Rosenberg, J. T. (1969). Shock compression of feldspars. *Journal of Geophysical Research*, *74*, 2727–2746.
- Arndt, J., Hummel, W., & Gonzalez-Cabeza, I. (1982). Diaplectic Labradorite labradorite glass from the Manicouagan impact crater, : I—Physical properties, crystallization, structural and genetic implications. *Physics and Chemistry of Minerals*, *8*, 230–239.
- Beck, P., Gillet, P., El Goresy, A., & Mostefaoui, S. (2005). Timescales of shock processes in chondritic and martian Martian meteorites. *Nature*, *435*, 1071–1074. <https://doi.org/10.1038/nature03616>
- Benedix, G. K., & Hamilton, V. E. (2007). Infrared (2.5 to 14 μm) reflectance microspectroscopy of meteoritic minerals in thin section, Lunar Plan. Sci. Conf. XXXVIII, abstract 1805.
- Bischoff, A., & Stöfler, D. (1992). Shock metamorphism as a fundamental process in the evolution of planetary bodies: Information from meteorites. *European Journal of Mineralogy*, *4*, 707–755.
- Bunch, T. E., Cohen, A. J., & Dence, M. R. (1967). Natural terrestrial maskelynite. *American Mineralogist*, *52*, 244–253.
- Bunch, T. E., Cohen, A. J., & Dence, M. R. (1968). Shock-induced structural disorder in plagioclase and quartz, in *Shock Metamorphism of Natural Materials*, Proc. First Conf., Mono Book Corp., Baltimore, 509–518.
- Chen, J., Jolliff, B. L., Wang, A., Korotev, R. L., Wang, K., Carpenter, P. K., et al. (2019). Petrogenesis and shock metamorphism of basaltic lunar meteorites Northwest Africa 4734 and 10597. *Journal of Geophysical Research, Planets*, *124*, 2583–2598. <https://doi.org/10.1029/2019JE006084>
- Christensen, P. R., Bandfield, J. L., Hamilton, V. E., Howard, D. A., Lane, M. D., Piatek, J. L., et al. (2000). A thermal emission spectral library of rock-forming minerals. *Journal of Geophysical Research*, *105*, 9735–9739.
- Cooney, T. F., Scott, E. R. D., Krot, A. N., Sharma, S. K., & Yamaguchi, A. (1999). Vibrational spectroscopic study of minerals in the Martian meteorite ALH84001. *American Mineralogist*, *84*, 1569–1576.
- Daniel, I., Gillet, P., & Ghose, S. (1995). A new high-pressure phase transition in anorthite (CaAl₂Si₂O₈) revealed by Raman spectroscopy. *American Mineralogist*, *80*, 645–648.
- Daniel, I., Gillet, P., McMillan, P. F., Wolf, G., & Verhelst, M. A. (1997). High-pressure behavior of anorthite: Compression and amorphization. *Journal of Geophysical Research*, *102*, 10,313–10,325.
- DeCarli, P. S., Bowden, E., Jones, A. P., & Price, G. D. (2002). Laboratory impact experiments versus natural impact events. In K. Coeberl & K. G. MacLeod (Eds.), *Catastrophic Events and Mass Extinctions: Impacts and Beyond, Special Paper* (Vol. 356, pp. 595–605). Boulder, CO: Geological Society of America.

- Dence, M. R., Grieve, R. A. F., & Robertson, P. B. (1977). Terrestrial impact structures: Principal characteristics and energy considerations. In D. J. Roddy, R. O. Pepin, & R. B. Merrill (Eds.), *Impact and Explosion Cratering* (pp. 247–275). New York: Pergamon Press.
- Dominguez, G., McLeod, A. S., Gainsforth, Z., Kelly, P., Bechtel, H. A., Keilmann, F., et al. (2014). Nanoscale infrared spectroscopy as a non-destructive probe of extraterrestrial samples. *Nature Communications*, 5, 5544.
- Farrell-Turner, S., Reimold, W. U., Nieuwoudt, M., & Erasmus, R. M. (2005). Raman spectroscopy of olivine in dunite experimentally shocked to pressures between 5 and 59 GPa. *Meteoritics & Planetary Science*, 40, 1311–1327. <https://doi.org/10.1111/j.1945-5100.2005.tb00403.x>
- Fernandes, V. A., Burgess, R., & Morris, A. (2009). 40Ar-39Ar age determinations of lunar basalt meteorites Asuka 881757, Yamato 793169, Miller Range 05035, La Paz Icefield 02205, Northwest Africa 479, and basaltic breccia Elephant Moraine 96008. *Meteoritics & Planetary Science*, 44, 805–821. <https://doi.org/10.1111/j.1945-5100.2009.tb00770.x>
- Fernandes, V. A., Fritz, J., Weiss, B. P., Garrick-Bethell, I., & Shuster, D. L. (2013). The bombardment history of the Moon as recorded by 40Ar-39Ar chronology. *Meteoritics and Planetary Science*, 48, 241–269. <https://doi.org/10.1111/maps.12054>
- Filiberto, J., Gross, J., Udry, A., Trela, J., Wittmann, A., Cannon, K. M., et al. (2018). Shergottite Northwest Africa 6963: A pyroxene-cumulate Martian gabbro. *Journal of Geophysical Research: Planets*, 123, 1823–1841. <https://doi.org/10.1029/2018JE005635>
- Foucher, F., Guillaume, G., Bost, N., & Westall, F. (2017). *Petrographical and mineralogical applications of Raman mapping, Raman spectroscopy and applications* (pp. 163–180). London: IntechOpen.
- Freeman, J. J., Wang, A., Kuebler, K., Jolliff, B. L., & Haskin, L. A. (2008). Characterization of natural feldspars by raman Raman spectroscopy for future planetary exploration. *The Canadian Mineralogist*, 46, 1477–1500.
- Fritz, J., Assis Fernandes, V., Greshake, A., Holzwarth, A., & Böttger, U. (2019). On the formation of diaplectic glass: Shock and thermal experiments with plagioclase of different chemical compositions. *Meteoritics and Planetary Science*, 54, 1533–1547. <https://doi.org/10.1111/maps.13289>
- Fritz, J., Greshake, A., & Fernandes, V. A. (2017). Revising the shock classification of meteorites. *Meteoritics and Planetary Science*, 52(6), 1216–1232. <https://doi.org/10.1111/maps.12845>
- Fritz, J., Greshake, A., & Stöffler, D. (2005). Micro-Raman spectroscopy of plagioclase and maskelynite in Martian meteorites: Evidence of progressive shock metamorphism. *Antarctic Meteorite Research*, 18, 96–116.
- Fritz, J., Wunnemann, K., Greshake, A., Fernandes, V. A. S. M., Boettger, U., & Hornemann, U. (2011). Shock pressure calibration for lunar plagioclase, Lunar Plan. Sci. Conf. 42, abstract #1196
- Gibbons, R. V., & Ahrens, T. J. (1971). Shock metamorphism of silicate glasses. *Journal of Geophysical Research*, 76(23), 5489–5498.
- Gibbons, R. V., Morris, R. V., Hörz, F., & Thompson, T. D. (1975). Petrographic and ferromagnetic resonance studies of experimentally shocked regolith analogs, Proc. Lunar Sci. Conf. 6th, 3143-3171.
- Glotch, T. D., & Ferrari, M. J. (2011). Raman microscopy of shocked and unshocked basalts from Lunar Crater, India, CORALS II Conference, abstract #4049.
- Glotch, T. D., & Rogers, A. D. (2013). Evidence for magma-carbonate interaction beneath Syrtis Major, Mars. *Journal of Geophysical Research: Planets*, 118, 126–137. <https://doi.org/10.1029/2012JE004230>
- Glotch, T.D., S.P. Wright, B.E. McKeeby, and M.J. Ferrari, Micro-FTIR and Micro-Raman spectroscopy of shocked basalts from Lunar Cratercrater, India, Lunar Plan. Sci. Conf. 42, abstract 1566, 2011.
- Glotch, T. D., Young, J. M., Yao, Z., Bechtel, H. A., Hamilton, V. E., Christensen, P. R., & Lauretta, D. S. (2019). Near-field infrared spectroscopy as a tool for analysis of chondritic returned samples, Asteroid Science in the Age of Hayabusa2 and OSIRIS-REx Workshop, abstract 2061.
- Grieve, R. A. F., Langenhorst, F., & Stöffler, D. (1996). Shock metamorphism of quartz in nature and experiment: II. Significance in geoscience. *Meteoritics and Planetary Science*, 31, 6–35.
- Gucsik, A., Koeberl, C., Brandstätter, F., Libowitzky, E., & Zhang, M. (2004). Infrared, Raman, and cathodoluminescence studies of impact glasses. *Meteoritics & Planetary Science*, 39(8), 1273–1285. <https://doi.org/10.1111/j.1945-5100.2004.tb00946.x>
- Gyollai, I., Gucsik, A., Nagy, S., & Bérczi, S. (2012). Petrographic and mid-infrared spectroscopy study of shocked feldspar in the Asuka-881757 Lunar gabbro meteorite sample. *Central European Geology*, 55(1), 23–32.
- Hans, R. E., Montague, B. R., Davis, M. K., Galindo, C., & Hörz, F. (1978). X-ray diffractometer studies of shocked minerals, Proc. Lunar Planet. Sci. Conf. 9th, 2773-2787.
- Harriss, K. H., & Burchell, M. J. (2016). A study of the observed shift in the peak position of olivine Raman spectra as a result of shock induced by hypervelocity impacts. *Meteoritics & Planetary Science*, 51(7), 1289–1300.
- Herd, C. D., Walton, E. L., Agee, C. B., Muttik, N., Ziegler, K., Shearer, C. K., et al. (2017). The Northwest Africa 8159 martian Martian meteorite: Expanding the martian Martian sample suite to the early Amazonian. *Geochimica et Cosmochimica Acta*, 218, 1–26.
- Heymann, D., & Hörz, F. (1990). Raman-spectroscopy and X-ray diffractometer studies of experimentally produced diaplectic feldspar glass. *Physics and Chemistry of Minerals*, 17, 38–44.
- Hirata, N., Kurita, K., & Sekine, T. (2009). Simulation experiments for shocked primitive materials in the solar system. *Physics of the Earth and Planetary Interiors*, 174, 227–241.
- Hörz, F., & Cintala, M. (1997). Impact experiments related to the evolution of planetary regoliths. *Meteoritics and Planetary Science*, 32, 179–209.
- Iiishi, K., Tomisaka, T., & Kato, T., Umegaki, Y. (1971). Isomorphous substitution and infrared and far infrared spectra of the feldspar group, Neues Jahrbuch fuer Mineralogie. Abhandlungen, 115, 98-119.
- Jaret, S. J., Glotch, T. D., & Wright, S. P. (2013). Micro-FTIR and Micromicro-Raman spectroscopy of a shocked basalt from the Lunar Cratercrater, India. 44th Lunar and Planetary Science Conference, LPI Contribution No. 1719, p.2881
- Jaret, S. J., Johnson, J. R., Sims, M., DiFrancesco, N., & Glotch, T. D. (2018). Microspectroscopic and petrographic comparison of experimentally shocked albite, andesine, and bytownite. *Journal of Geophysical Research: Planets*, 123, 1701–1722. <https://doi.org/10.1029/2018JE005523>
- Jaret, S. J., Johnson, J. R., Sims, M., & Glotch, T. D. (2018). A Micromicro-spectroscopic comparison of experimentally shocked basalts, Lunar and Plan. Sci. Conf., abstract #2355.
- Johnson, J. R. (2012). Thermal infrared spectra of experimentally shocked andesine anorthosite. *Icarus*, 221, 359–364. <https://doi.org/10.1016/j.icarus.2012.08.012>
- Johnson, J. R., Hörz, F., Christensen, P., & Lucey, P. G. (2002). Thermal infrared spectroscopy of experimentally shocked anorthosite and pyroxenite: Implications for remote sensing of Mars. *Journal of Geophysical Research*, 107(E10), 5073. <https://doi.org/10.1029/2001JE001517>

- Johnson, J. R., Hörz, F., & Staid, M. I. (2003). Thermal infrared spectroscopy and modeling of experimentally shocked plagioclase feldspars. *American Mineralogist*, *88*, 1575–1582.
- Johnson, J. R., Staid, M. I., & Kraft, M. D. (2007). Thermal infrared spectroscopy and modeling of experimentally shocked basalts. *American Mineralogist*, *92*, 1148–1157.
- Johnson, J. R., Staid, M. I., Titus, T. N., & Becker, K. (2006). Shocked plagioclase signatures in Thermal Emission Spectrometer data of Mars. *Icarus*, *180*, 60–74.
- Kebukawa, Y., Kobayashi, H., Urayama, N., Baden, N., Kondo, M., Zolensky, M. E., & Kobayashi, K. (2019). Nanoscale infrared imaging analysis of carbonaceous chondrites to understand organic-mineral interactions during aqueous alteration. *Proceedings of the National Academy of Sciences*, *116*, 753–758.
- Kubo, T., Kimura, M., Kato, T., Nishi, M., Tominaga, A., Kikegawa, T., & Funakoshi, K. I. (2010). Plagioclase breakdown as an indicator for shock conditions of meteorites. *Nature Geoscience*, *3*(1), 41.
- Lyon, R. J. P. (1963). Evaluation of infrared spectrophotometry for compositional analysis of lunar and planetary soils, NASA Tech. Note D-1871.
- Manzari, P., De Angelis, S., De Sanctis, M. C., Agrosi, G., & Tempesta, G. (2019). Microimaging spectroscopy and scanning electron microscopy of Northwest Africa 8657 shergottite: Interpretation of future in situ Martian data. *Meteoritics & Planetary Science*, *54*(3), 475–494.
- Martin, D. J. P., Leivia, A., Bell, S. K., Pernet-Fisher, J. F., Joy, K. H., Morlok, A., et al. (2018). Investigating the orientation of minerals using FTIR microspectroscopy. Proceedings of the 49th Lunar and Planetary Science Conference Abstract 2138.
- Melosh, H. J. (1989). *Impact Cratering: A Geologic Process*. New York, NY: Oxford University Press.
- Mernagh, T. P. (1991). Use of the laser raman Raman microprobe for discrimination amongst feldspar minerals. *Journal of Raman Spectroscopy*, *22*, 453–457.
- Morlok, A., Bowey, J., Kokler, M., & Grady, M. M. (2006). FTIR 2-16 micron spectroscopy of micron-sized olivines from primitive meteorites. *Meteoritics and Planetary Science*, *41*, 773–784.
- Morlok, A., Kohler, M., Bowey, J. E., & Grady, M. M. (2006). FT-IR microspectroscopy of extraterrestrial dust grains: Comparison of measurement techniques. *Planetary and Space Science*, *54*, 599–601.
- Morlok, A., Koike, C., Tomioka, N., Mann, I., & Tomeoka, K. (2010). Mid-infrared spectra of the shocked Murchison CM chondrite: Comparison with astronomical observations of dust in debris disks. *Icarus*, *207*, 45–53.
- Neal, C. R., Donohue, P., Fagan, A. L., O'Sullivan, K., Oshrin, J., & Roberts, S. (2015). Distinguishing between basalts produced by endogenic volcanism and impact processes: A non-destructive method using quantitative petrography of lunar basaltic samples. *Geochimica et Cosmochimica Acta*, *148*, 62–80.
- Osinski, G. R., & Pierazzo, E. (2013). *Impact Cratering Processes and Products* (p. 360). New York: Wiley-Blackwell. <https://doi.org/10.1002/9781118447307.ch1>
- Ostertag, R. (1983). Shock experiments on feldspar crystals, Proc. 14th Lunar Plan. Sci. Conf. *Journal of Geophysical Research*, *88*, B364–B376.
- Palomba, E., Rotundi, A., & Colangeli, L. (2006). Infrared micro-spectroscopy of the Martian meteorite Zagami: Extraction of individual mineral phase spectra. *Icarus*, *182*, 68–79.
- Pernet-Fisher, J. F., Joy, K. H., Martin, D. J. P., & Donaldson Hanna, K. L. (2017). Assessing the shock state of the lunar highlands: Implications for the petrogenesis and chronology of crustal anorthosites. *Scientific Reports*, *7*, 5888.
- Pickersgill, A. E., Flemming, R. L., & Osinski, G. R. (2015). Toward quantification of strain-related mosaicity in shocked lunar and terrestrial plagioclase by in situ micro-X-ray diffraction. *Meteoritics and Planetary Science*, *50*, 1–12. <https://doi.org/10.1111/maps.12514>
- Pickersgill, A. E., Osinski, G. R., & Flemming, R. L. (2015). Shock effects in plagioclase feldspar from the Mistastin Lake impact structure, Canada. *Meteoritics and Planetary Science*, *50*, 1546–1561. <https://doi.org/10.1111/maps.12495>
- Prinsloo, L. C., Colombari, P., Brink, J. D., & Meiklejohn, I. (2011). A Raman spectroscopic study of the igneous rocks on Marion Island: A possible terrestrial analogue for the geology on Mars. *Journal of Raman Spectroscopy*, *42*(4), 626–632.
- Reimold, W. U. (1982). The Lappajärvi meteorite crater, Finland: petrography, Rb-Sr, major and trace element geochemistry of the impact melt and basement rocks. *Geochimica et Cosmochimica Acta*, *46*, 1203–1225.
- Rogers, A. D. (2011). Crustal compositions exposed by impact craters in the Tyrrhena Terra region of Mars: Considerations for Noachian environments. *Earth and Planetary Science Letters*, *301*(1-2), 353–364.
- Rogers, A. D., & Aharonson, O. (2008). Mineralogical composition of sands in Meridiani Planum determined from Mars Exploration Rover data and comparison to orbital measurements. *Journal of Geophysical Research*, *113*, E06S14. <https://doi.org/10.1029/2007JE002995>
- Rubin, A. E. (2015). Maskelynite in asteroidal, lunar and planetary basaltic meteorites: An indicator of shock pressure during impact ejection from their parent bodies. *Icarus*, *257*, 221–229.
- Ruff, S. W., Christensen, P. R., Blaney, D. L., Farrand, W. H., Johnson, J. R., Michalski, J. R., et al. (2006). The rocks of Gusev cCrater as viewed by the Mini-TES instrument. *Journal of Geophysical Research*, *111*, E12S18. <https://doi.org/10.1029/2006JE002747>
- Sazonova, L., Kozlov, E., & Zhugin, Yu. (1996). Transformations of quartz-plagioclase-garnet-clinopyroxene rock in spherical stress waves, Lunar Planet. Sci. Conf. XXVII, 1135–1136.
- Sazonova, L. V., Milyavskii, V. V., Borodina, T. I., Sokolov, S. N., & Zhuk, A. Z. (2007). Shock metamorphism of plagioclase and amphibole (experimental data). *Izvestiya, Physics of the Solid Earth*, *43*, 707–712.
- Sharp, T. G., & DeCarli, P. S. (2006). Shock effects in meteorites, in *Meteorites and the Early Solar System II*, p. 653–677.
- Sharp, T. G., Walton, E. L., Hu, J., & Agee, C. (2019). Shock conditions recorded in NWA 8159 martian augite basalt with implications for the impact cratering history on Mars. *Geochimica et Cosmochimica Acta*, *246*, 197–212.
- Short, N. M. (1970). Progressive shock metamorphism of quartzite ejecta from the Sedan nuclear explosion crater. *Journal of Geology*, *78*, 705–732.
- Sims, M., Jaret, S. J., Carl, E., Rhymer, B., Schrodt, N., Mohrholz, V., et al. (2019). Pressure-induced amorphization in plagioclase feldspars: A time-resolved powder diffraction study during rapid compression. *Earth and Planetary Science Letters*, *507*, 166–174.
- Stöffler, D. (1971). Progressive metamorphism and classification of shocked and brecciated crystalline rocks at impact craters. *Journal of Geophysical Research*, *76*, 5541–5551.
- Stöffler, D. (1972). Deformation and transformation of rock-forming mineral by natural and experimental shock processes I. Behavior of minerals under shock compression. *Fortschritte der Mineralogie*, *49*, 50–113.
- Stöffler, D. (1974). Deformation and transformation of rock-forming minerals by natural and experimental shock processes, II. Physical properties of shocked minerals. *Fortschritte der Mineralogie*, *51*, 256–289.

- Stöffler, D. (2001). Maskelynite confirmed as diaplectic glass: Indication for peak shock pressures below 45 GPa in all Martian meteorites, Lunar Plan. Sci. Conf. XXXII, Abs. #1170.
- Stöffler, D., Hamann, C., & Metzler, K. (2018). Shock metamorphism of planetary silicate rocks and sediments: Proposal for an updated classification system. *Meteoritics & Planetary Science*, 53(1), 5–49.
- Stöffler, D., & Hornemann, U. (1972). Quartz and feldspar glasses produced by natural and experimental shock. *Meteoritics*, 7, 371–394.
- Stöffler, D., Keil, K., & Scott, E. (1991). Shock metamorphism of ordinary chondrites. *Geochimica et Cosmochimica Acta*, 55, 3845–3867.
- Stöffler, D., & Langenhorst, F. (1994). Shock metamorphism of quartz in nature and experiment: I. Basic observation and theory. *Meteoritics*, 29, 155–181.
- Thoma, K., Hornemann, U., Sauer, M., & Schneider, E. (2005). Shock waves—Phenomenology, experimental, and numerical simulation. *Meteoritics and Planetary Science*, 40, 1283–1298.
- Trepman, C. A. (2008). Shock effects in quartz: Compression versus shear deformation—An example from the Rouchouart impact structure, France. *Earth and Planetary Science Letters*, 267, 322–332.
- Velde, B., Syono, Y., Couty, R., & Kikuchi, M. (1987). High pressure infrared spectra of diaplectic anorthite glass. *Physics and Chemistry of Minerals*, 14, 345–349.
- Velde, B., Syono, Y., Kikuchi, M., & Boyer, H. (1989). Raman microprobe study of synthetic diaplectic plagioclase feldspars. *Physics and Chemistry of Minerals*, 16, 436–441.
- Wang, A., Jolliff, B. L., & Haskin, L. A. (1995). Raman spectroscopy as a method for mineral identification on lunar robotic exploration missions. *Journal of Geophysical Research*, 100(E10), 21,189–21,199. <https://doi.org/10.1029/95JE02133>
- Wang, A., Jolliff, B. L., Haskin, L. A., Kuebler, K. E., & Viskupic, K. M. (2001). Characterization and comparison of structural and compositional features of planetary quadrilateral pyroxenes by Raman spectroscopy. *American Mineralogist*, 86(7–8), 790–806.
- Wang, A., Korotev, R. L., Jolliff, B. L., & Ling, Z. (2015). Raman imaging of extraterrestrial materials. *Planetary and Space Science*, 112, 23–34.
- Williams, Q. (1998). High-pressure infrared spectra of feldspars: Constraints on compressional behavior, amorphization, and diaplectic glass formation. In M. H. Manghni & T. Yagi (Eds.), *Properties of Earth and Planetary Material at High Pressure and Temperature, Geophys. Monograph* (Vol. 101, pp. 531–543). Washington, DC: American Geophysical Union.
- Williams, Q., & Jeanloz, R. (1988). Spectroscopic evidence for pressure-induced coordination changes in silicate glasses and melts. *Science*, 239, 902–905.
- Williams, Q., & Jeanloz, R. (1989). Static amorphization of anorthite at 300 K and comparison with diaplectic glass. *Nature*, 338, 413–415.
- Yamaguchi, A., & Sekine, T. (2000). Monomineralic mobilization of plagioclase by shock: An experimental study. *Earth and Planetary Science Letters*, 175, 289–296.
- Zeng, X., Li, X., Martin, D., Tang, H., Yu, W., Liu, J., & Wang, S. (2019). Micro-FTIR spectroscopy of lunar pyroclastic and impact glasses as a new diagnostic tool to discern them. *Journal of Geophysical Research: Planets*, 124, 3267–3282. <https://doi.org/10.1029/2019JE006237>
- Zhang, B., Shieh, S. R., Withers, A. C., & Bouvier, A. (2018). Raman spectroscopy of shocked enstatite-rich meteorites. *Meteoritics & Planetary Science*, 53(10), 2067–2077.